



# Simulated solvation of organic ions II: Study of linear alkylated

Céline Houriez, Meot-Ner Michael, Michel Masella

► **To cite this version:**

Céline Houriez, Meot-Ner Michael, Michel Masella. Simulated solvation of organic ions II: Study of linear alkylated. *Journal of Physical Chemistry B*, American Chemical Society, 2015, 119, pp.12094-12107. <10.1021/acs.jpbc5b04556>. <hal-01254502>

**HAL Id: hal-01254502**

**<https://hal-mines-paristech.archives-ouvertes.fr/hal-01254502>**

Submitted on 12 Jan 2016

**HAL** is a multi-disciplinary open access archive for the deposit and dissemination of scientific research documents, whether they are published or not. The documents may come from teaching and research institutions in France or abroad, or from public or private research centers.

L'archive ouverte pluridisciplinaire **HAL**, est destinée au dépôt et à la diffusion de documents scientifiques de niveau recherche, publiés ou non, émanant des établissements d'enseignement et de recherche français ou étrangers, des laboratoires publics ou privés.

1 **Simulated solvation of organic ions II: Study of linear alkylated**  
2 **carboxylate ions in water nanodrops and in liquid water.**  
3 **Propensity for air/water interface and convergence to bulk**  
4 **solvation properties**

5 Céline Houriez,<sup>1</sup> Michael Meot-Ner (Mautner),<sup>2</sup> and Michel Masella<sup>3</sup>

6 *<sup>1</sup>MINES ParisTech, PSL Research University,*

7 *CTP - Centre Thermodynamique des Procédés,*

8 *35 rue Saint-Honoré, 77300 Fontainebleau, France*

9 *<sup>2</sup>Department of Chemistry, Virginia Commonwealth University, Richmond,*

10 *Virginia 23284-2006, United States, and Department of Chemistry,*

11 *University of Canterbury, Christchurch, New Zealand 8001*

12 *<sup>3</sup>Laboratoire de Biologie Structurale et Radiobiologie,*

13 *Service de Bioénergétique, Biologie Structurale et Mécanismes,*

14 *Institut de Biologie et de Technologies de Saclay,*

15 *CEA Saclay, F-91191 Gif sur Yvette Cedex, France*

## Abstract

We investigated the behavior of six linear alkylated carboxylate ions, from methanoate (formate) to hexanoate, in small water droplets comprising from 50 to 1000 water molecules or in neat water, by a computational protocol based on standard molecular dynamics schemes and on sophisticated polarizable models to handle both ion/water and water/water interactions. Our results show that in small droplets all of the alkylated carboxylate ions from methanoate to hexanoate present a strong propensity for the air/water interface. This propensity is lowered as the droplet size increases, so that only carboxylate ions larger than propanoate still have a noticeable propensity for the interface, in agreement with recent experimental findings. For these larger ions, transfer to the surface reduces enthalpic stabilization by ion/water dispersion effects in the interior by 3 kcal mol<sup>-1</sup> per methylene (CH<sub>2</sub>) group, similar to hydrophobic solvation effects from cluster-based analysis. However, this is compensated by entropy effects of > +3.3 cal mol<sup>-1</sup> K<sup>-1</sup> per CH<sub>2</sub> group. These effects in the model reproduce the known structure-making effects of the alkyl groups in solution, and their loss upon transfer to the surface. There the carboxylate ion headgroups are strongly oriented near the air/water interface with the anionic head pointing towards the aqueous core, while the hydrophobic alkyl chains are repelled into air and desolvate, losing their structure-making effects. Further, comparison with alkylammonium ions shows that the hydrocarbon chains of anions and cations solvate similarly, and the ionic headgroups and alkyl substituents solvate as independent solutes. From droplet data, we estimated the carboxylate single absolute solvation enthalpies using standard extrapolation schemes. For the two smallest carboxylate ions, the results yield an absolute proton solvation enthalpy close to the experiment-based value, similar to the value reported in our former study dealing with methylated ammonium ions (about 270 kcal mol<sup>-1</sup>). However, the extrapolated proton solvation enthalpy for the largest carboxylate ions is smaller by about 10 kcal mol<sup>-1</sup>. The origin of this discrepancy will have to be investigated by much larger droplets whose simulations are still demanding.

**Keywords.** Organic ion solvation, carboxylate ions, molecular dynamics, droplets, hydrophobic solvation, air/water interfaces.

## 43 I. INTRODUCTION

44 Ion behavior at aqueous interfaces is a major research field in physics, chemistry and  
45 biology. In particular, it drives many important atmospheric and environmental chemistry  
46 processes [2, 3]. It plays also a key role in understanding acid-base reactions at air/water  
47 interfaces that govern many important processes in the living cell, from enzyme cataly-  
48 sis to molecular recognition, and in understanding surfactants and self-assembly to form  
49 membranes, micelles and vesicles [4–7].

50 When considering organic ions, many of them contain both hydrophobic and hydrophilic  
51 moieties that modulate their hydration properties, as well as their behavior at air/water  
52 interfaces. Among these ions, alkylcarboxylate ions are of particular interest because (1)  
53 they are among the simplest ionic systems presenting both a hydrophilic anionic head and a  
54 hydrophobic alkyl side chain and (2) they are a major component of many biological macro-  
55 molecules (from proteins to cell membranes). We may also quote that these ions were  
56 shown to contribute significantly to the cloud droplet forming ability [8]. However, even for  
57 simple carboxylate ions solvated in bulk water, most of the experimental data reported to  
58 date focus on the hydration properties of their  $\text{COO}^-$  head [9–12], and only sparse data  
59 were reported concerning the effects of their hydrophobic moiety on their solvation process.  
60 This is in part due to similarity of the time scale of the water dynamics in the bulk and  
61 in the vicinity of small solutes (see among others the discussions provided in Refs. 13  
62 and 14). Nevertheless, by analyzing surface sensitive core-level electron spectra, Ottosson  
63 and coworkers [15] concluded recently that the propensity of alkylcarboxylate ions for the  
64 air/liquid water interface increases when lengthening their alkyl side chain and that only  
65 large enough alkylcarboxylate ions, starting at butanoate, have a noticeable propensity for  
66 this interface.

67 An alternative route to investigate the behavior of ions in aqueous media and at inter-  
68 faces is to consider computer simulations at the microscopic level. For instance, several  
69 studies concerning the behavior of carboxylate ions both in neat water and at the air/liquid  
70 water interface have been reported. To perform reliable simulations of organic ions, accu-  
71 rate computational protocols able to simulate both water/water and ion/water interactions  
72 are needed. However, the most sophisticated protocols, based for instance on DFT molec-  
73 ular dynamics or on hybrid QM/MM approaches, are highly computationally demanding.

74 That explains why they were used to investigate only the smallest carboxylate ions, namely  
75  $\text{HCOO}^-$  and  $\text{CH}_3\text{COO}^-$ , solvated in liquid water [16–18]. Only a few studies were devoted  
76 to theoretically investigate complex aqueous solutions involving carboxylate ions or the be-  
77 havior of carboxylate ions at the air/liquid water interface. Most of them were based on  
78 efficient but simple pairwise forcefields [19–23], and we may quote only a few attempts to  
79 use sophisticated polarizable approaches to investigate the hydration of the  $\text{COO}^-$  moiety,  
80 as in simple organic ions [24], in the glycine zwitterion and in the aspartylalanine dipep-  
81 tide [25]. However, many authors [26–30] pronounced it necessary to explicitly considering  
82 microscopic polarization effects in simulating the propensity of polarizable ions, like car-  
83 boxylates, for the air/water interface. Moreover, all the standard pairwise water forcefields  
84 used up to now to simulate organic ions in bulk water are known for their poor ability to  
85 describe water aggregates in gas phase (cf. the discussions in Ref. [31], for instance). Hence,  
86 simulating carboxylate hydration process by sophisticated and accurate polarizable models  
87 may provide new and useful data for interpreting experiments. That will help also to assess  
88 the ability of commonly used standard pairwise forcefields to model the hydration of single  
89 or multiple ions not only in the bulk phase but also in droplets [32].

90 The aim of the present work is to investigate the behavior of six small linear alkylated  
91 carboxylate ions, from methanoate to hexanoate, in small water droplets, comprising from  
92 50 to 1000 water molecules, and in neat water. To this end, we use sophisticated polariz-  
93 able models to handle both ion/water and water/water interactions, namely the water rigid  
94 model TCPE/2013 [33] and a  $\text{COO}^-$ /water model similar to the recent one proposed to  
95 model halide hydration [34]. These two approaches were shown to accurately model pure  
96 water and halide/water systems in the gas phase as well as in the bulk. We use the same com-  
97 putational protocol based on standard molecular dynamics schemes as in our recent study  
98 dealing with the solvation of methylated ammonium ions in water nanodroplets [35]. The  
99 present study focuses mainly on evaluating the effects both of the alkyl side chain length and  
100 of the droplet size on the propensity of carboxylate ions for the air/water interface. Here,  
101 we investigate only the solvation of a single carboxylate anion in a pure water environment  
102 without considering any acid association/dissociation phenomena at the air/water interface,  
103 for which many conflicting results have been reported (see the recent discussions in Ref.  
104 [36]). Note that our simulation protocol will yield equilibrium thermochemistry values (like  
105 ion/water and water/water interaction enthalpies) which are independent of other equilibria

106 that the species participate in. Among the ion solvation properties, we mainly focus our  
 107 analyses on the possible change in the carboxylate structure and orientation when crossing  
 108 the air/water interface, and on the single carboxylate ion absolute solvation enthalpies esti-  
 109 mated from droplet data, by using four different extrapolation schemes based on power-law  
 110 functions of the droplet size. Previously, we considered only one fitting function in our  
 111 study about methylated ammonium ions. For the sake of comparison, we thus extrapolate  
 112 here again the solvation enthalpies of these cations using the four extrapolation schemes to  
 113 further discuss their ability in providing reliable results.

## 114 II. THEORETICAL METHODS

115 In the following,  $N$  is the total number of atoms considered,  $M$  is the total number of  
 116 atoms in an ion,  $N_\mu$  is the total number of polarizable atoms,  $N_w$  is the total number of  
 117 water molecules and  $M_w$  is the total number of atoms belonging to the water molecules.  
 118 All molecular modeling computations were performed with our own code POLARIS(MD)  
 119 as in our former study regarding ammonium ions [35]. All quantum computations were  
 120 performed by means of the GAUSSIAN09 package of programs [37], using the frozen core  
 121 approximation systematically.

### 122 A. The model

123 The total potential energy  $U$  of a carboxylate/water system, *i.e.* the energy of the  
 124 reaction  $n\text{H}_2\text{O} + \text{carboxylate} \rightarrow \text{carboxylate}/(\text{H}_2\text{O})_n$ , is decomposed into three terms: the  
 125 ion internal energy  $U^{rel}$ , and the ion/water  $U^{iw}$  and water/water  $U^{ww}$  interaction energies.

126 As in our former study concerning ammonium ions [35], we consider here the rigid water  
 127 model TCPE/2013 [33]. Besides the repulsive and Coulombic energy terms ( $U^{rep}$  and  $U^{qq'}$ ),  
 128 TCPE/2013 also includes a polarization energy term  $U^{pol}$  (based on an induced point dipole  
 129 moment approach) and a short-range anisotropic many-body energy term  $U^{hb}$  to accurately  
 130 reproduce hydrogen bond (HB) network properties. Analytically, the term  $U^{hb}$  is close to  
 131  $U^{shb}$  used to model carboxylate/water interactions (see below). The sum of the four terms,

$$U^{ww} = U^{rep} + U^{qq'} + U^{pol} + U^{hb}, \quad (1)$$

132 gives the total potential energy of a pure molecular water system, with respect to individual  
 133 unbound gas phase molecules. TCPE/2013 is shown to model accurately liquid water over  
 134 a wide range of thermodynamic conditions, as well as water clusters in gas phase and the  
 135 water interactions in cation first hydration shells [33]. For systems composed of anions like  
 136  $\text{Br}^-$  and  $\text{I}^-$  interacting directly with 4 to 8 water molecules, TCPE/2013 is also shown to  
 137 reproduce high level quantum computation results concerning the water interaction energies,  
 138 within 1 kcal mol<sup>-1</sup> on average [38].

139 The carboxylate/water energy term  $U^{iw}$  is the sum of six terms:

$$U^{iw} = U^{rep} + U^{qq'} + U^{pol} + U^{disp} + U^{shb} + U^{rel}. \quad (2)$$

140 The repulsive  $U^{rep}$ , Coulombic  $U^{qq'}$ , and dispersion  $U^{disp}$  terms are defined as

$$U^{rep} = \sum_{i=1}^M \sum_{j=1}^{M_w} a_{ij} \exp(-b_{ij} r_{ij}), \quad (3)$$

141

$$U^{qq'} = \sum_{i=1}^M \sum_{j=1}^{M_w} \frac{q_i q_j}{4\pi\epsilon_0 r_{ij}}, \quad (4)$$

142

$$U^{disp} = - \sum_{i=1}^M \sum_{j=1}^{M_w} \left( \frac{r_{ij}^*}{r_{ij}} \right)^6. \quad (5)$$

143 Here,  $r_{ij}$  is the distance between the atoms  $i$  and  $j$ ,  $q_i$  are the static charges located on  
 144 atomic centers, and  $a_{ij}$ ,  $b_{ij}$  and  $r_{ij}^*$  are adjustable parameters. The repulsive term  $U^{rep}$  is  
 145 truncated for distances larger than 5.0 Å. Dispersion effects are accounted for by considering  
 146 only interactions between water oxygen atoms and carbon atoms. The energy term  $U^{rel}$   
 147 is introduced to handle the intramolecular degrees of freedom of the carboxylate ion. It  
 148 includes standard stretching, bending and torsional terms, as well as an improper torsional  
 149 term  $U^{imp} = \frac{1}{2} k_{imp} \psi^2$ , where  $\psi$  is the improper dihedral angle  $\angle \text{OC}_1\text{C}_2\text{O}$  (see Figure 1 for  
 150 labelling).

151 The polarisation energy term  $U^{pol}$  including both ion/water and water/water interactions  
 152 is defined as

$$U^{pol} = \frac{1}{2} \sum_{i=1}^{N_\mu} \frac{p_i^2}{\alpha_i} - \sum_{i=1}^{N_\mu} \mathbf{p}_i \cdot \mathbf{E}_i^q - \frac{1}{2} \sum_{i=1}^{N_\mu} \sum_{j=1}^{N_\mu^*} \mathbf{p}_i \mathbf{T}_{ij} \mathbf{p}_j. \quad (6)$$

153 Here, the superscript \* indicates that the corresponding sum includes only pairs of atoms  
 154 separated by more than two chemical bonds. Only non-hydrogen atoms are considered as

155 polarizable centers, with an isotropic polarizability  $\alpha_i$  and an induced dipole moment  $\mathbf{p}_i$   
 156 given by

$$\mathbf{p}_i = \alpha_i \cdot \left( \mathbf{E}_i^q + \sum_{j=1}^{N_\mu^*} \mathbf{T}_{ij} \cdot \mathbf{p}_j \right). \quad (7)$$

157  $\mathbf{T}_{ij}$  is the dipolar interaction tensor and  $\mathbf{E}_i^q$  is the electric field generated on the polar-  
 158 izable center  $i$  by the surrounding static charges  $q_j$ .  $\mathbf{T}_{ij}$  and  $\mathbf{E}_i^q$  both include an inter-  
 159 molecular short-range damping component, corresponding to a radial charge distribution  
 160  $\rho(r) \propto \exp(-c \times r^3)$ , with  $c$  a parameter and  $r$  the distance from an atomic center [39].

161 Lastly, we consider also the many-body anisotropic short-range energy term  $U^{shb}$ , which  
 162 was recently proposed to model halide/water interactions [33]:

$$U^{shb} = \sum f(r)g(\psi). \quad (8)$$

163 The sum runs over all the carboxylate/water strong hydrogen bonds (SHB).  $f$  and  $g$  are  
 164 Gaussian functions:

$$f(r) = D_e \exp \left[ -\frac{(r_{shb} - r_{e,shb})^2}{\gamma_r} \right] \quad \text{and} \quad g(\psi) = \exp \left[ -\frac{(\psi - \psi_e)^2}{\gamma_\psi} \right]. \quad (9)$$

165  $r_{shb}$  is the SHB length and  $\psi$  is the O-H $\cdots$ O<sub>carboxylate</sub> angle.  $r_{e,shb}$  and  $\psi_e$  are their  
 166 equilibrium values. To account for the chemical environment effect on the strength of a  
 167 local SHB,  $D_e$  is taken as a linear function of the local density of water O-H bonds,  $\rho_{oh}$ ,  
 168 in the anion vicinity:  $D_e = d_e(1 - \xi\rho_{oh})$ , with  $d_e$  and  $\xi$  two adjustable parameters.  $\rho_{oh}$  is  
 169 estimated according to

$$\rho_{oh} = \sum \exp \left[ -\frac{(r_{shb} - r_{e,shb})^2}{\gamma'_{rt}} \right]. \quad (10)$$

170 Here, the sum runs over all the water/carboxylate SHB, apart from the local one consid-  
 171 ered explicitly in the present function  $f$ .  $\gamma'_{rt}$  is a parameter adjusted to take into account  
 172 mainly the water molecules of the first hydration shell of the COO<sup>-</sup> moiety (here,  $\gamma'_{rt}$  is set  
 173 to 0.3 Å).  $U^{shb}$  is smoothly zeroed between  $r_{shb}$  distances of 5.5 and 6.0 Å, using a fifth order  
 174 spline function.

175 Originally,  $U^{shb}$  was used to account for the charge transfer effects occurring in halide/water  
 176 SHB [34]. In the present study, it is introduced to destabilize a particular CH<sub>3</sub>COO<sup>-</sup>/(H<sub>2</sub>O)<sub>2</sub>  
 177 trimer structure, labelled **2-0** in Figure 1. MP2/aug-cc-pVTZ quantum computations show  
 178 this structure to be unstable, since it evolves towards the structure **2-1** during the geometry  
 179 optimization process. By considering only the five other energy terms of  $U^{iw}$ , we were not



180 able to destabilize this particular structure **2-0** while this can be readily done by using the  
181  $U^{shb}$  term with an anti-cooperative parameter  $\xi < 0$ . We may note here that the formation  
182 of anti-cooperative SHBs between the carboxylate moiety and water molecules was recently  
183 invoked to interpret experimental infrared spectroscopy data concerning the carboxylate  
184 group hydration [9].

185 To assign the  $U^{iw}$  parameters, we consider as reference data the quantum results con-  
186 cerning eight small  $\text{CH}_3\text{COO}^-/(\text{H}_2\text{O})_n$  clusters ( $n=1-4$ ). Their geometries were optimized  
187 at the MP2/aug-cc-pVTZ level. The cluster binding energies ( $\text{BE}_n$ ) were estimated at the  
188 complete basis set (CBS) limit, according to the same computational protocol as in Ref.  
189 35. To assign the charges of the  $\text{COO}^-$  moiety, we consider the quantum Natural Popu-  
190 lation Analysis results concerning the isolated ion  $\text{CH}_3\text{COO}^-$ , and the charges of the side  
191 chain methylene groups were assigned according to the same protocol as in our former study  
192 dealing with methylated ammonium ions [35]. The isotropic atomic polarizabilities for the  
193 carboxylate oxygen and carbon atoms were assigned to reproduce the molecular polarizabil-  
194 ity of  $\text{CH}_3\text{COO}^-$  computed at the MP2/aug-cc-pVQZ level ( $4.9 \text{ \AA}^3$ ), and knowing our earlier  
195 value for methyl carbon ( $2.1 \text{ \AA}^3$ ). We assume here that the polarizabilities of the  $\text{COO}^-$   
196 moiety atoms are close to each other. Lastly, from our computations, it appears that the  
197 polarization damping effects don't play a pivotal role to reproduce accurately the quantum  
198  $\text{BE}_n$ . The damping parameters  $c$  are thus chosen to make the carboxylate/water damping  
199 effects small (i.e.  $c = 0.3 \text{ \AA}^{-3}$ ).

200 The torsional parameters corresponding to all the carboxylate dihedral angles, like  
201  $\angle\text{OCCH}$  or  $\angle\text{CCCC}$ , were assigned to reproduce at best the quantum energy profiles of  
202 these angles computed at the MP2/aug-cc-pVTZ level, and by considering all the other  
203 model parameters defined as above. In particular, these torsional parameters allow one to  
204 reproduce the differences in energy among the different minima of the dihedral angle energy  
205 profiles. Lastly, all the other parameters of  $U^{rel}$  are taken from the CHARMM 2.7 forcefield  
206 [40].

207 Most of the above-mentioned quantum results, the carboxylate/water cluster structures  
208 and the  $U^{iw}$  parameter set are provided as Supporting Information. The optimum parameter  
209 set allows one to reproduce the cluster SHB lengths within less than  $0.05 \text{ \AA}$  on average and  
210 the quantum CBS  $\text{BE}_n$  within less than  $0.75 \text{ kcal mol}^{-1}$  on average (the  $\text{BE}_n$  range from 20  
211 to  $67 \text{ kcal mol}^{-1}$  for  $n=1-4$ ).

212 **B. Simulation details**

213 MD simulations of carboxylate/water droplet systems and of carboxylate molecules at  
 214 the air/liquid water interface are performed in the NVT ensemble. Bulk carboxylate/water  
 215 systems are simulated in the NPT ensemble. Bulk and air/liquid water interface systems  
 216 include about 1000 and 2000 water molecules, respectively. The simulation duration is 10  
 217 ns and all the trajectories are sampled each 1 ps. The potentials of mean force (PMF)  
 218 corresponding to the interaction of a carboxylate ion with a water system (droplet or liquid  
 219 water) are computed according to a standard umbrella sampling protocol. The degree of  
 220 freedom constrained during these simulations,  $d$ , is either the distance between the carbon  
 221 atom of the  $\text{COO}^-$  moiety and the droplet center of mass (COM), or the projection of the  
 222 distance between the carboxylate carbon and the simulation cell center (SCC) on the axis  
 223 orthogonal to the air/liquid water interface. The details of these protocols are provided as  
 224 Supporting Information. The target value of the  $d$  along an umbrella sampling simulation  
 225 is denoted  $d_c$ .

226 While no truncation is applied to the different energy terms in droplet simulations (with  
 227 the exception of  $U^{rep}$  and  $U^{shb}$ ), ion/water dispersion interactions are truncated in sim-  
 228 ulations of the bulk phase and of the air/liquid water interface for distances larger than  
 229  $R_{\text{cutoff}} = 12 \text{ \AA}$  (corresponding to the cutoff value for the Ewald direct energy terms used  
 230 to simulate liquid water systems). Hence, for comparison purposes with droplet results,  
 231 the PMF computed from bulk simulations have to be corrected to account for the disper-  
 232 sion truncation. For the present discussions, we only apply such a correction to the PMF  
 233 minimum values observed close to the air/liquid water interface (see below), by adding the  
 234 following amount of energy to the PMF values:

$$\delta\text{PMF} = \int_{R_{\text{cutoff}}}^{\infty} - \sum \left( \frac{r_{ij}^*}{r} \right)^6 \times 4\pi r^2 \rho_s dr = \frac{4\pi\rho_s}{3R_{\text{cutoff}}^3} \times \sum (r_{ij}^*)^6. \quad (11)$$

235 The sum runs over all the carboxylate dispersion centers and  $\rho_s$  is the solvent density (taken  
 236 as a constant and equal to the water bulk density,  $0.0331 \text{ molecule \AA}^{-3}$ ). This represents  
 237 the upper limit of the amount of energy not accounted for in bulk simulations when using a  
 238 cutoff to handle ion/water dispersion. The magnitude of  $\delta\text{PMF}$  ranges from 0.11 ( $\text{HCOO}^-$ )  
 239 to  $0.39 \text{ kcal mol}^{-1}$  ( $\text{C}_5\text{H}_{11}\text{COO}^-$ ).

240 To minimize the impact of evaporation phenomena in the droplet simulations, we used

241 the same computational protocol as in our ammonium study [35]. Droplet systems are  
242 confined in a spherical cavity, whose radius corresponds to the largest droplet COM/water  
243 oxygen distance to which 12 Å are added. As a water molecule crosses the cavity boundary,  
244 it undergoes a reflexion from a perfect elastic collision with the cavity wall. With such a  
245 protocol, we showed that the total number of interacting water molecules in a droplet differs  
246 on average by 0.3 molecules from the total number of water molecules  $N_w$  along the 10  
247 ns ion/droplet simulations, leading to an uncertainty affecting the water/water interaction  
248 energy of 5 kcal mol<sup>-1</sup> at most [35].

### 249 III. RESULTS AND DISCUSSION

#### 250 A. Carboxylate molecules in gas and liquid phases

##### 251 1. Carboxylate structures in gas phase

252 Here, we discuss the most stable carboxylate structures in gas phase, in terms of dihedral  
253 angles  $\angle C_n C_{n+1} C_{n+2} C_{n+3}$ , whose values are denoted by  $\Psi_{n+3}$  (see Figure 1). The most stable  
254 carboxylate conformations were identified by performing 1 ns simulations in gas phase at a  
255 constant temperature of 300 K, and by systematically quenching the trajectories each 1 ps.

256 For the hexanoate, the most stable structure predicted by our model is shown in Figure  
257 1. The  $\Psi_{n+3}$  values are 67, 50 and 178° for  $n = 1 - 3$ , respectively. The  $\Psi_{n+3}$  values given  
258 by our model for the most stable butanoate and pentanoate structures are in line with the  
259 hexanoate ones. For instance, in the case of the butanoate, the angles  $\Psi_4$  and  $\Psi_5$  are of 69  
260 and 60°, respectively. Hence, our model predicts the dihedral angles close to the carboxylate  
261 anionic head to be in a gauche conformation, while a dihedral anti conformation is observed  
262 for methyl groups distant by more than 3 carbon atoms from the COO<sup>-</sup> moiety. This result  
263 agrees with our quantum computations concerning the propanoate and the butanoate (see  
264 the dihedral energy profiles provided as Supporting Information). Note that the  $\Psi_{n+3}$  values  
265 are 52, 57 and 177° in the optimized structure of pentanoate, obtained from MP2/aug-cc-  
266 pVDZ quantum computations, and by considering as starting point the most stable structure  
267 given by our model. From the crystallographic structures of the Cambridge Structural  
268 Database (CSD) [41], a gauche conformation for the dihedral angle  $\Psi_4$  is observed in 30% of  
269 the CSD structures for both pentanoate and hexanoate and between 30% (pentanoate) and

270 15% (hexanoate) for  $\Psi_5$ . For the hexanoate  $\Psi_6$  angle, less than 10% of the CSD structures  
271 are in a gauche conformation. Keeping in mind the constraints occurring in the solid phase,  
272 our model data are in a reasonable agreement with the CSD ones for the latter dihedral  
273 angles.

274 Lastly, for the forthcoming discussions of Section III C, the distances between the carbon  
275 atoms of the  $\text{COO}^-$  and  $\text{CH}_3$  moieties in the most stable gas phase carboxylate structures  
276 are 1.5, 3.3, 3.9 and 4.9 Å from ethanoate to hexanoate, respectively.

## 277 2. Solvent structure in the vicinity of carboxylate ions in liquid water

278 To assess the reliability of our model to simulate the hydration process of carboxylate  
279 ions in large water systems, we discuss here the water structure in the vicinity of the  $\text{COO}^-$   
280 moiety in the liquid phase, observed along the NPT bulk simulations. Moreover, we compare  
281 our results to earlier data computed from QM/MM hybrid and Car-Parrinello simulations  
282 [16–18], as well as to experiments [9–12].

283 Figure 2 shows the radial distribution functions computed along the bulk simulations,  
284 and corresponding to  $\text{COO}^-$  oxygen/water oxygen [ $g_{\text{OO}_w}(r)$ ],  $\text{COO}^-$  carbon/water oxygen  
285 [ $g_{\text{CO}_w}(r)$ ], and  $\text{COO}^-$  oxygen/water hydrogen [ $g_{\text{OH}_w}(r)$ ]. The first peak positions of our three  
286 kinds of distribution functions are located around 2.70, 3.60 and  $1.70 \pm 0.05$  Å, regardless of  
287 the carboxylate ion. For the alkylated carboxylate ions, the first minima of the distribution  
288 functions are located around 3.50, 4.10 and  $2.45 \pm 0.05$  Å for  $g_{\text{OO}_w}(r)$ ,  $g_{\text{CO}_w}(r)$  and  $g_{\text{OH}_w}(r)$ ,  
289 and the coordination numbers are  $3.1 \pm 0.1$  and  $3.2 \pm 0.1$ , and  $7.8 \pm 0.2$  for the two oxygen  
290 atoms and the carbon atom of the  $\text{COO}^-$  moiety, respectively. Regarding the functions  
291  $g_{\text{OO}_w}(r)$  and  $g_{\text{OH}_w}(r)$ , the profiles of their first peak are similar for all the carboxylate ions.  
292 This result was expected, as the first peaks correspond to the direct interactions of water  
293 molecules with the  $\text{COO}^-$  moiety, which are slightly influenced by the carboxylate aliphatic  
294 chain.

295 The main features of all these distribution functions are in line with those derived from  
296 QM/MM simulations with several DFT levels of theory concerning  $\text{HCOO}^-$  and  $\text{CH}_3\text{COO}^-$   
297 in neat water [17, 18]. For instance, for  $\text{HCOO}^-$ , the positions of the first peaks were found  
298 to be 2.67–2.76 Å for  $g_{\text{OO}_w}(r)$  and 1.71–1.84 Å for  $g_{\text{OH}_w}(r)$  [17]. For  $\text{CH}_3\text{COO}^-$ , the first  
299 peaks are located around 2.66–2.74 Å for  $g_{\text{OO}_w}(r)$ , 3.50–3.60 Å for  $g_{\text{CO}_w}(r)$ , and 1.67–1.78

300 Å for  $g_{\text{OH}_w}(r)$ , and the corresponding coordination numbers are 2.9–3.0 per  $\text{COO}^-$  oxygen,  
 301 and 7.6–8.3 for the  $\text{COO}^-$  carbon [18]. Our results are also in very good agreement with  
 302 those obtained from classical MD and Monte Carlo simulations with pairwise or polarizable  
 303 forcefields [19, 20, 24]. In all of these studies, the first peaks of the radial distribution func-  
 304 tions are located around 2.7, 3.7, and 1.7 Å for  $g_{\text{OO}_w}(r)$ ,  $g_{\text{CO}_w}(r)$ , and  $g_{\text{OH}_w}(r)$ , respectively.  
 305 The coordination numbers per carboxylate oxygen are found to be 3.6 in the case of  $\text{HCOO}^-$   
 306 [20] and around 3.4 for  $\text{CH}_3\text{COO}^-$  [19, 20, 24].

307 For the  $g_{\text{OO}_w}(r)$  second peak, its height decreases as we lengthen the carboxylate side  
 308 chain. This result originates from the side chain steric effect that prevents water molecules  
 309 to interact in the direction of the carboxylate  $\text{OOC} - \text{R}$  axis ( $\text{R} = \text{H}, \text{C}$ ). Hence, more water  
 310 molecules are allowed to interact at short range with the  $\text{COO}^-$  carbon for the smallest  
 311 carboxylate ions than for the larger ones. That also explains the different properties of the  
 312 function  $g_{\text{CO}_w}(r)$  for  $\text{HCOO}^-$ , relative to alkylated carboxylates. For instance, in the case  
 313 of  $\text{HCOO}^-$ , the height of the  $g_{\text{CO}_w}(r)$  first peak is 2.8 and the first minimum is around 4.5  
 314 Å while the corresponding values for alkylated ions are about 2.3 and 4.1 Å. That yields a  
 315 coordination number for the  $\text{HCOO}^-$  carbon atom almost twice larger than for the alkylated  
 316 carboxylate ions, respectively 13.5 and 7.8.

317 Experimentally, the hydration number per  $\text{COO}^-$  oxygen ranges from 1.2 to 4.5 (see  
 318 among others Refs. 13, 14, and 42 and the references cited therein). Such a large range  
 319 of values originates from both the different experimental conditions used and the different  
 320 definitions considered for the hydration number, preventing a direct comparison with the-  
 321 oretical estimates. Nevertheless, our computed hydration numbers for the  $\text{COO}^-$  oxygen  
 322 atoms agree with the most accepted experimental values, ranging from 2.5 to 3.0.

### 323 3. Bulk water destabilization and ion deformation energies

324 Besides the ion/water interaction energies, two other important quantities have to be  
 325 taken into account to investigate the energetics of the ionic solvation process: the bulk water  
 326 destabilization energies  $\Delta\bar{U}_{\text{bulk}}^{ww}$  due to the ion presence and the intramolecular deformation  
 327 energies  $\Delta\bar{U}_{\text{intra}}^{\text{ion}}$  between gas phase and solution for polyatomic ions.

328 We estimated the water destabilization energies by comparing the water/water interaction  
 329 energies from simulations of neat water and of an hydrated ion. The ion intramolecular

330 deformation energies were computed from the sets of ion coordinates extracted from bulk  
 331 simulations. The corresponding averaged energies are then subtracted from the isolated ion  
 332 energies at  $T = 300$  K, computed from 1 ns gas phase simulations.  $\Delta\bar{U}_{\text{bulk}}^{ww}$  and  $\Delta\bar{U}_{\text{intra}}^{\text{ion}}$  are  
 333 summarized in Table II for the carboxylates and for the methylated ammonium ions and  
 334  $\text{K}^+$ , as computed from the data of our former study [35]. Concerning the latter cations, the  
 335 water destabilization energies  $\Delta\bar{U}_{\text{bulk}}^{ww}$  were computed in our previous study from simulations  
 336 performed using classical Ewald summation techniques for neat water and the Particle Mesh  
 337 Ewald method for ionic solutions. The values reported here correspond to data computed  
 338 using the same Particle Mesh Ewald protocol. That explains the weak differences in values  
 339 of Table II for the cations, relative to the original values [35].

340 The deformation energies  $\Delta\bar{U}_{\text{intra}}^{\text{ion}}$  are small for all the ions. They are at most of about 1  
 341 kcal mol<sup>-1</sup> for the largest carboxylates while they are all negligible for the cations and the  
 342 smallest carboxylates ( $< 0.3$  kcal mol<sup>-1</sup>). Similar to the methylated ammonium ions [35],  
 343 the water destabilization energies  $\Delta\bar{U}_{\text{bulk}}^{ww}$  are very similar for all the carboxylates (around  
 344  $47.0 \pm 0.7$  kcal mol<sup>-1</sup>). This result will be further discussed below.

## 345 B. Probability of ion location and ion/water PMF at air/water interfaces

346 The ion/water PMF relates to the ion/water system partition function  $Z$

$$Z \propto \int \exp[-\text{PMF}(d)/k_B T] dv. \quad (12)$$

347 Here,  $d$  corresponds either to the distance  $r$  between the carbon atom of the  $\text{COO}^-$  moiety  
 348 and the droplet COM, or to the projection  $z$  of the distance between this carbon atom and  
 349 the cell center on the axis orthogonal to the interface, when simulating air/liquid water  
 350 interfaces. As in the case of the ammonium/water droplets, the carboxylate ions interact  
 351 with quasi-spherical droplets, regardless of the droplet size and of the carboxylate. Hence,  
 352  $dv \propto r^2 dr$  for ion/water droplet systems and  $dv \propto dz$  for air/liquid water systems.

353 For air/liquid water systems, the probability density of finding an ion at a position  $z$  is

$$P(z) = \exp[-\text{PMF}(z)/k_B T] / Z. \quad (13)$$

354 By considering the entropic term  $\text{TS}_{\text{geom}}(r) = k_B T \ln(r^2)$ , the probability density  $P(r)$  of  
 355 finding an ion at a distance  $r$  from the droplet COM is

$$P(r) = \exp\{-[\text{PMF}(r) - \text{TS}_{\text{geom}}(r)]/k_B T\} / Z. \quad (14)$$

356 The PMF for carboxylate/droplet systems are shown in Figure 3. The corresponding  
 357 density probabilities  $P(r)$  and the air/liquid water PMFs are provided as Supporting Infor-  
 358 mation. The entropic term  $TS_{geom}(r)$  represents the larger accessible volume as the distance  
 359  $r$  increases for a quasi spherical droplet. It plays a noticeable role when  $PMF(r)$  is flat  
 360 enough, as for the present carboxylate ions, *i.e.* it drives the ions towards the interface. For  
 361 instance, in the case of  $N_w = 1000$  droplet systems, by estimating the mean distance  $r$  from  
 362 probability densities computed by accounting for it or not (these densities are both provided  
 363 as Supporting Information), we show that this entropic term is responsible for an increase  
 364 of the mean distance  $r$  by about 3-4 Å for carboxylates with a strong interface propensity,  
 365 and up to 6-8 Å for carboxylates with a weak interface propensity (namely  $HCOO^-$  and  
 366  $CH_3COO^-$ ). Moreover, this entropic term is also at the origin of an excluded volume (cor-  
 367 responding to weak  $P(r)$  values) observed at the center of all the droplets, even for the  
 368 anions showing the weakest propensity for the droplet surface, such as  $HCOO^-$ . However,  
 369 this volume decreases rapidly as the droplet size increases. For instance, in the case of the  
 370  $HCOO^-/N_w = 1000$  droplet system, the volume of the sphere centered at the droplet COM  
 371 and within which the ion location probability  $P(r)$  is 10 times smaller than the maximum  
 372 of  $P(r)$ , represents less than 3% of the total droplet volume.

373 All the ion/water PMFs have a local minimum close to the air/water interface (usually  
 374 at about 2 Å from the interface, within the droplet). Such a minimum was also observed for  
 375 methylated ammonium ions while it doesn't exist for monoatomic cations like  $K^+$  [35]. We  
 376 interpret it here as the first step of the solvation process of an organic ion, corresponding  
 377 to the saturation of the first hydration shell of its ionic head while its alkyl groups are  
 378 still weakly interacting with water (see also Figure 5). This interpretation explains why  
 379 this minimum is located at the same distance from the interface for all the carboxylates  
 380 considered. The PMF values for these minima,  $PMF_{min}$ , are plotted as a function of the  
 381 droplet size in Figure 4. For  $N_w > 50$  and for all the carboxylates, the  $PMF_{min}$  value  
 382 increases with the droplet size and it rapidly converges towards its value at the air/liquid  
 383 water interface, the convergence being almost achieved for  $N_w = 1000$ . For  $N_w \leq 100$ , the  
 384  $PMF_{min}$  values are all negative, showing the strong propensity of all the carboxylates for  
 385 the surface of small droplets. The carboxylate ions alter thus noticeably the structure of  
 386 their surrounding water, which prevents them to easily penetrate in small droplets. For  
 387 the largest carboxylates, the propensity for the droplet surface remains strong up to the

388 air/liquid water interface (for both  $C_4H_9COO^-$  and  $C_5H_{11}COO^-$ , their  $PMF_{min}$  values are  
389 then around  $-1.5 \text{ kcal mol}^{-1}$ ) while the surface propensity of the smallest carboxylates,  
390  $HCOO^-$  to  $C_2H_5COO^-$ , disappears as soon as  $N_w = 300$ . This is in line with a recent  
391 experimental study [15] showing that only carboxylate ions larger than propanoate have a  
392 marked propensity for the air/liquid water interface.

393 The solvation of carboxylate ions is mainly driven by rather strong electrostatic water/ $COO^-$   
394 interactions. However, the marked difference in propensity for the interface between small  
395 and large alkylated carboxylates solvated in large water systems shows the pivotal role that  
396 a few methyl groups can play on organic ion solvation properties. As the destabilization  
397 of the water structure due to the presence of such small hydrophobic groups is overall  
398 weak (the hydration free energy of methane is  $+2 \text{ kcal mol}^{-1}$ ), this demonstrates that the  
399 competition between ion/water and water/water interactions can be easily altered. We may  
400 note here that the interaction energy profile for a small ion solvated in water is flat (see for  
401 instance our former results for  $NH_4^+$  [35], as well as the below-discussed ones corresponding  
402 to  $HCOO^-$ ). This suggests the air/water interface propensity of an organic ion to be mainly  
403 dominated by ion carbon chain/water hydrophobic effects. That explains why the trends of  
404 the carboxylate propensity for the air/liquid water interface predicted by our simulations  
405 is in line with the solvation trends of neutral hydrocarbons (see for instance the recent dis-  
406 cussion of Ben-Amotz [43]). In other words, the present study suggests that the ionic head  
407 and the alkyl substituent of an organic ion can be considered as solvated independently.

408 We note a very good agreement between the  $PMF_{min}$  values corresponding to droplets  
409 with  $N_w = 1000$  and to air/liquid water interfaces, for the four smallest carboxylates while  
410 these values differ by about  $0.4 \text{ kcal mol}^{-1}$  for the largest carboxylates  $C_4H_9COO^-$  and  
411  $C_5H_{11}COO^-$ . This difference may originate from the correction  $\delta PMF$  used to account for  
412 the dispersion truncation in bulk simulations, which is estimated by using a basic relation  
413 not suited for large polyatomic ions (see Section II B). However, this may also result from  
414 small differences in the large carboxylate structures in the interface vicinity between droplet  
415 and bulk systems, even if we have not been able to identify them because of the too large  
416 statistical uncertainty still affecting data extracted from 10 ns-scale simulations (see below).



417 **C. Carboxylate orientation at the air/water interface**

418 To investigate the effects of solvation on the orientation and on the structure of alkylated  
 419 carboxylates, especially in the vicinity of the air/water interfaces, we consider two main  
 420 kinds of geometric parameters, namely the distances  $R_C$  between the carbon atom of the  
 421 carboxylate  $\text{CH}_3$  group and the droplet COM (or simulation cell SCC) in large water systems,  
 422 and the carboxylate dihedral angles  $\Psi_n$ . Below, the intramolecular axis between the carbon  
 423 atoms of the  $\text{COO}^-$  and of the  $\text{CH}_3$  moieties is denoted by  $\mathbf{L}_{CC}$ . Its norm in gas phase is  
 424 denoted by  $L_{CC}$ , and its values are 1.5, 3.3, 3.9 and 4.9 Å from ethanoate to hexanoate,  
 425 respectively (see Section III A 1).

426 For the  $N_w = 1000$  droplet systems (radii around 20 Å), the averaged quantities  $\Delta\bar{R}_C =$   
 427  $\bar{R}_C - d_c$  and the root mean square deviations  $\delta\bar{R}_C$  of  $R_C$  are plotted vs. the distances  $d_c$   
 428 in Figure 6. These profiles are very close to the profiles computed at the air/liquid water  
 429 interface (see Supporting Information). Regardless of the carboxylate ion, we identify two  
 430 main regimes for  $\Delta\bar{R}_C$ . In the vicinity of the droplet core, the orientation of  $\mathbf{L}_{CC}$  is random  
 431 ( $\Delta\bar{R}_C \approx L_{CC}$  at the droplet core, i.e., when  $d_c = 0$ ) and then, it decreases down to zero  
 432 as  $d_c$  increases. However, starting at about 10 Å before the air/water interface, the axis  
 433  $\mathbf{L}_{CC}$  is more and more oriented orthogonally to the interface, i.e.,  $\Delta\bar{R}_C$  converges towards  
 434 a maximum value (around  $+L_{CC}$ ) reached about 4-5 Å before the interface. Close to the  
 435 air/water interface, the carboxylate orientation is thus strongly constrained. The  $\text{COO}^-$   
 436 moiety points towards the aqueous core while the alkyl chain is repelled from it. As shown  
 437 by the  $\delta\bar{R}_C$  plots, this structural constraint is particularly strong in a shell of 3 Å before the  
 438 droplet boundary for all the alkylcarboxylates (in this domain,  $\delta\bar{R}_C \leq 2$  Å).

439 Some examples of distributions of the dihedral angles  $\Psi_n$ ,  $g_{\Psi_n}$ , computed along sim-  
 440 ulations at the air/liquid water interface are provided as Supporting Information for the  
 441 hexanoate. For all of the carboxylates, the  $g_{\Psi_n}$  functions present three sharp peaks at 120,  
 442 180 and 240°, allowing one to compute the ratios  $p_{\Psi_n}$  between anti and gauche conforma-  
 443 tions, for each dihedral angle  $\Psi_n$ . These ratios computed from air/liquid water simulation  
 444 data are plotted vs.  $d_c$  for the three largest carboxylates in Figure 7. Profiles very close to  
 445 the latter ones are computed from  $N_w = 1000$  droplet data (see Supporting Information).  
 446 First, by comparing the  $p_{\Psi_n}$  values within the bulk and in the gas phase (but far from  
 447 the air/water interface), they seem to be still affected by relatively large uncertainties, as

448 shown by the marked discontinuous profiles of  $p_{\Psi_n}$ . These statistical uncertainties prevent  
 449 us to discuss the possible weak structural changes affecting large carboxylates when crossing  
 450 air/water interfaces. Nevertheless, the hexanoate  $p_{\Psi_n}$  profiles show that the carboxylate  
 451 dihedral angles  $\Psi_5$  and  $\Psi_6$  (corresponding exclusively to methyl carbon atoms) are slightly  
 452 altered when crossing the air/water interface while the dihedral angle  $\Psi_4$  (whose first carbon  
 453 atom belongs to the  $\text{COO}^-$  moiety) is more sensitive to the solvent effects. For instance, the  
 454 ratio  $p_{\Psi_4}$  increases from about 1:6 in gas phase to 1:4 in the bulk, with a maximum of 1:3  
 455 in the vicinity of the air/water interface for hexanoate, showing that the anti conformation  
 456 for  $\Psi_4$  is favored by the solvent effects. For such a large anion, that may be interpreted  
 457 as allowing more water molecules to interact with the carboxylate anionic head in solution.  
 458 However, the dependence of dihedral angles  $\Psi_4$  on the chemical environment seems to be  
 459 less accented for the smallest carboxylate ions (see for instance the profiles plotted in Figure  
 460 7 for pentanoate).

#### 461 **D. Microscopic interactions occurring in ion solvation**

462 Along each umbrella sampling simulation, we computed the ion/water mean energy  
 463  $\bar{U}^{iw}(d_c)$  and its components  $\bar{U}_{rep}^{iw}(d_c)$ ,  $\bar{U}_{qq'}^{iw}(d_c)$ ,  $\bar{U}_{pol}^{iw}(d_c)$ ,  $\bar{U}_{shb}^{iw}(d_c)$  and  $\bar{U}_{disp}^{iw}(d_c)$ , as well as  
 464 the water/water interaction mean energy  $\bar{U}^{ww}(d_c)$ . The results for ions in  $N_w = 600$  water  
 465 droplets, as a function of ion/COM distance  $d_c$ , are illustrated in Figure 8 for six carboxylate  
 466 ions. As in the case of ammonium ions and for all the droplet systems, the root mean square  
 467 deviation of  $\bar{U}^{iw}(d_c)$  is about 6 kcal mol<sup>-1</sup> and the uncertainty affecting the  $\bar{U}^{ww}(d_c)$  values  
 468 and tied to droplet evaporation effects is at most 5 kcal mol<sup>-1</sup>. Below, we denote by  $\bar{U}_{xx}^{yy}$  the  
 469 average of the energy component  $\bar{U}_{xx}^{yy}(d_c)$  scaled by the probability density  $P(d_c)$  of finding  
 470 an ion at a position  $d_c$  during a simulation.

471 The  $\bar{U}_{qq'}^{iw}(d_c)$  and  $\bar{U}_{shb}^{iw}(d_c)$  profiles in Figure 8 are very similar for all the alkylated car-  
 472 boxylates. This result was expected for  $\bar{U}_{shb}^{iw}(d_c)$ , as it corresponds to a short-range energy  
 473 term centered on the  $\text{COO}^-$  oxygen atoms. For the Coulombic components  $\bar{U}_{qq'}^{iw}(d_c)$ , that  
 474 arises from the strong electrostatic charges located on the  $\text{COO}^-$  moiety, which mainly drive  
 475 the Coulombic ion/water interactions (we assume that the charges on the  $\text{COO}^-$  oxygens  
 476 are equal for all of the carboxylate ions).

477 Ion/water dispersion becomes stronger when the carboxylate side chain is longer. Each

478 added methylene group adds an ion/water dispersion energy  $\bar{U}_{disp}^{iw}(d_c)$  of  $-3 \text{ kcal mol}^{-1}$ .  
 479 Similarly, the ion/water repulsion and the water/water energies  $U_{rep}^{iw}(d_c)$  and  $U_{ww}(d_c)$  also  
 480 change regularly with each new methylene group but oppositely, with a destabilizing effect,  
 481 each adding a positive interaction energy of  $1 \text{ kcal mol}^{-1}$  per group. Lastly, the ion/water  
 482 polarization destabilizes (increases the energy) the ion/water interactions within a droplet.  
 483 The strength of this destabilization also increases with the alkyl chain length, adding  $+0.6$   
 484  $\text{kcal mol}^{-1}$  per  $\text{CH}_2$  group, but not linearly as for ion/water repulsion. In particular,  $U_{pol}^{iw}(d_c)$   
 485 seems to already converge for pentanoate.

486 For  $\bar{U}_{disp}^{iw}(d_c)$ , the stabilization of  $-3 \text{ kcal mol}^{-1}$  per added  $\text{CH}_2$  group may result from  
 487 two weak  $\text{CH} \cdots$  solvent hydrogen bond interactions (thus of  $-1.5 \text{ kcal mol}^{-1}$ ). This effect is  
 488 comparable, within the usual  $1 \text{ kcal/mol}$  uncertainty of these estimates, to the cluster-based  
 489 analysis for alkyloxonium and alkylammonium ions, where each  $\text{CH} \cdots$  solvent interaction  
 490 adds about  $-2.5 \text{ kcal mol}^{-1}$  to the hydrophobic solvation enthalpy (i.e., each  $\text{CH}_2$  group  
 491 adds  $-5 \text{ kcal mol}^{-1}$ )[44, 45]. This similarity suggests that  $\bar{U}_{disp}^{iw}(d_c)$  is a significant factor in  
 492 hydrophobic solvation. Interestingly, the similar effect for the onium cations and carboxylate  
 493 anions suggests then that the hydrophobic solvation energy per CH hydrogen may also apply  
 494 to the solvation of alkyl groups of alkylated neutral molecules.

495 As already reported in earlier studies [35, 46, 47], water molecules jump from the droplet  
 496 onto the ions at the water surface. That explains why the short-range ion/water energies  
 497 like  $\bar{U}_{rep}^{iw}(d_c)$  and  $\bar{U}_{shb}^{iw}(d_c)$  don't converge towards zero outside of the droplet. Concerning  
 498  $\text{HCOO}^-$ , most of its ion/water energy components behave as in the case of the alkylated  
 499 carboxylates. The differences between the  $\text{HCOO}^-$  and alkylated data may be interpreted  
 500 as resulting from the  $\text{HCOO}^-$  small size allowing more water molecules to interact with it  
 501 at short range.

502 Interestingly, the sum of the total ion/water and the water/water interaction energies  
 503  $\bar{U}^{iw}(d_c)$  and  $\bar{U}^{ww}(d_c)$  at the droplet core is very close regardless of the alkylated carboxylate  
 504 size, within less than  $2 \text{ kcal mol}^{-1}$  in the particular case of  $N_w = 600$  droplet systems for  
 505  $d_c < 8 \text{ \AA}$  (see Fig. 8). However, this sum is weaker and weaker as the anion size increases,  
 506 showing that enthalpic effects seem to favor the hydration of large carboxylates. Hence,  
 507 their larger propensity for the air/water interface, relative to the small carboxylates, has an  
 508 entropic origin (like the perturbation of water molecule HB networks at the vicinity of the  
 509 anion carbon chains [48]).

510 As for ammonium ions and  $K^+$ , and for all the carboxylates, Coulombic and dispersion  
 511 ion/water interactions are centripetal (as well as the specific carboxylate/water  $U_{shb}^{iw}$  term),  
 512 whereas ion/water polarization and repulsive effects are centrifugal. Moreover, the water  
 513 structure reorganization induced by the carboxylate ion presence leads also to centrifugal  
 514 forces, as in the ammonium and  $K^+$  case. That shows the ion solvation process to be  
 515 controlled by the same microscopic forces, regardless of the nature of the ion. In particular,  
 516 ion/water polarization effects systematically disadvantage ion solvation inside the droplets  
 517 and favors the ionic interface propensity. That clearly shows the necessity to accurately  
 518 model ion/water polarization for a proper description of ions at air/water interfaces, in  
 519 agreement with earlier findings [28–30]. Nevertheless, the weights of the different ion/water  
 520 interaction terms can largely differ according to the ion nature. For instance, if all the  
 521 water/water interaction energies  $\bar{U}^{ww}$  are less stable in ion/droplet systems than in pure  
 522 water droplets, the water destabilization energies (i.e., the differences in the  $\bar{U}^{ww}$  energies  
 523 between ion/droplet and pure water droplet systems) are larger for carboxylates than for  
 524 ammonium ions, by 50% (about 15 kcal mol<sup>-1</sup>).

### 525 E. Effects of hydrocarbon chain lengths on solvation enthalpies and entropies

526 The incremental effects of added CH<sub>2</sub> groups on ion solvation enthalpies can be evaluated  
 527 quantitatively by comparing for example the shortest and longest alkylated carboxylates in  
 528 Figure 8 (i.e. ethanoate and hexanoate interacting with a 600 water droplet). Note that  
 529 even if the uncertainty affecting the water/water interaction enthalpies is about 5 kcal mol<sup>-1</sup>  
 530 because of evaporation effects (see above), the smoothed water/water interaction enthalpies  
 531 shown in Figure 8 can be considered reliable within about  $\pm 1$  kcal mol<sup>-1</sup>. Moreover, the  
 532 values discussed below agree with those computed from 1000 water droplet data within less  
 533 than 1 kcal mol<sup>-1</sup>.

534 Figure 8A shows that the total ion/water interaction enthalpy  $U_{iw}$  near the droplet COM  
 535 for hexanoate is more negative by 5 kcal mol<sup>-1</sup> than for ethanoate, i.e.,  $\Delta U_{iw}(\text{hex-eth}) = -5$   
 536 kcal mol<sup>-1</sup>. However, the water/water interaction enthalpy difference varies oppositely, as  
 537  $\Delta U_{ww}(\text{hex} - \text{eth}) = + 3$  kcal mol<sup>-1</sup>. Hence the difference between the solvation enthalpies  
 538 of hexanoate and ethanoate inside the droplet is then  $\Delta U_{sol}^{\text{COM}}(\text{hex} - \text{eth}) = \Delta U_{iw}(\text{hex-eth})$   
 539  $+ \Delta U_{ww}(\text{hex} - \text{eth}) = -2$  kcal mol<sup>-1</sup>. In comparison, the Figure 8 data at the droplet

540 surface lead to  $\Delta U_{iw}(\text{hex} - \text{eth}) = +2 \text{ kcal mol}^{-1}$  and to  $\Delta U_{ww}^{\text{surface}}(\text{hex} - \text{eth}) = 0$ . The total  
541 difference between the solvation enthalpies of hexanoate and ethanoate at the surface is thus  
542  $\Delta U_{\text{sol}v}^{\text{surface}}(\text{hex} - \text{eth}) = +2 \text{ kcal mol}^{-1}$ .

543 Hence, the total calculated solvation enthalpy is more negative (stabilizing) for hexanoate  
544 than for ethanoate by  $2 \text{ kcal mol}^{-1}$  inside the droplet, where the ionic groups and hydrocar-  
545 bon chains are fully solvated, while the solvation enthalpy is less stabilizing (more positive)  
546 for hexanoate than for ethanoate at the droplet surface by  $2 \text{ kcal mol}^{-1}$ . Hence, moving the  
547 anions from the droplet core to the droplet surface is more endothermic by  $4 \text{ kcal mol}^{-1}$  for  
548 hexanoate than for ethanoate. From the data summarized in Supporting Information, the  
549 latter difference is mainly due to methylene/water dispersion effects, in agreement with ear-  
550 lier studies showing that the electrostatic organic ion/water term does not vary significantly  
551 with alkyl size, but the solvation enthalpies of the neutrals does vary with alkyl size [49, 50].

552 By these enthalpy effects hexanoate should have a higher affinity for the interior than  
553 ethanoate. However, our simulations show that hexanoate has a higher propensity for the  
554 air/liquid water interface than ethanoate. That suggests thus an additional positive entropy  
555 effect in moving hexanoate from the droplet core to the droplet surface, to make the free  
556 energy of transfer to the surface negative (because of the PMF definition, see Equation  
557 `equ:prob-droplet`, this entropic effect is different from the  $TS_{\text{geom}}$  one discussed above).  
558 This new effect can be associated with the loss of structure-making effect of hydrocarbon  
559 solutes on surrounding water (here, structure-making  $\text{CH} \cdots \text{OH}_2$  hydrogen bonds in ion  
560 solvation lead to a compensating enthalpy/entropy effect common in thermochemistry).  
561 Quantitatively, the above results suggests that adding 4  $\text{CH}_2$  groups from ethanoate to  
562 hexanoate needs to contribute, for moving the ion to the surface, a desolvation entropic  
563 term  $T\Delta S_{\text{alkyl}}$  of  $> 4 \text{ kcal mol}^{-1}$ , or  $> 1 \text{ kcal mol}^{-1}$  per  $\text{CH}_2$  group (that corresponds to  
564 a solvation entropy change of  $< -3.3 \text{ cal mol}^{-1} \text{ K}^{-1}$  per  $\text{CH}_2$  group). The latter value is  
565 in line with the solvation entropy values reported experimentally for  $n$ -propanoate and  
566  $n$ -butanoate, which are more negative than ethanoate by  $-4.3$  and  $-7.7 \text{ cal mol}^{-1} \text{ K}^{-1}$  [50],  
567 respectively.

568 **F. Ion/water droplet solvation energy: convergence towards bulk limit**

569 The mean ion/water droplet energies  $\bar{U}^{iw}$  are plotted as a function of the droplet size  
 570  $N_w$  in Figure 9 for all the carboxylate ions. While they are all very similar for the smallest  
 571 droplet  $N_w = 50$ , their behavior differ then for the different carboxylates in larger droplets.  
 572 Nevertheless, we note that all of the values  $\bar{U}^{iw}$  for alkylated carboxylates seem to converge  
 573 towards the same value  $\bar{U}^{iw}(\infty)$  for  $N_w \rightarrow \infty$ . This convergence is a priori faster for  
 574 the smallest alkylated carboxylates. To extrapolate the value  $\bar{U}^{iw}(\infty)$  from quasi-spherical  
 575 droplet data for a small polyatomic ion, a standard approach consists in fitting the  $\bar{U}^{iw}(N_w)$   
 576 data to the power-law function of  $N_w$

$$\bar{U}^{iw}(N_w) = \bar{U}^{iw}(\infty) + \epsilon_0/(N_w + a)^{1/3} + \epsilon_1/(N_w + a)^{2/3}. \quad (15)$$

577 Here,  $\bar{U}^{iw}(\infty)$ ,  $\epsilon_0$ ,  $\epsilon_1$  and  $a$  are adjustable parameters. As all the water droplets are quasi-  
 578 spherical, the quantity  $(N_w + a)^{1/3}$  is a measure of the droplet radius  $R_d$ , and  $a$  is the ratio  
 579 between the ion effective volume and the solvent one. Lastly, the fourth term of Equation  
 580 15 is introduced to account for a non-symmetric charge distribution in an ion, like for the  
 581 carboxylates (see Figure 1). As discussed in Ref. 51 and for the droplet size considered here,  
 582 the above-mentioned equation can be used regardless of the ion propensity for the droplet  
 583 interior (or surface). However, because of the size of our droplet systems (their radii are at  
 584 most around 20 Å), this equation is expected to provide reliable results only for the smallest  
 585 carboxylates.

586 In our former study dealing with methylated ammonium cations and  $K^+$ , we extrapolated  
 587 the  $\bar{U}^{iw}(\infty)$  values by setting the parameters  $a$  and  $\epsilon_1$  to zero. To assess the reliability of  
 588 these former results and the ability of such a fitting function to extrapolate bulk values, we  
 589 fitted our former cation data and the carboxylate ones by considering three different kinds  
 590 of functions, for which the parameters  $a$  and  $\epsilon_1$  are set to zero individually or together. All  
 591 of the new extrapolated  $\bar{U}^{iw}(\infty)$  values are summarized in Table II.

592 For all the cations, the results summarized in Table II clearly show that the choice of  
 593 the fitting function has no effect on the extrapolated  $\bar{U}^{iw}(\infty)$  values, which differ in this  
 594 case by 1.2 kcal mol<sup>-1</sup> on average. For the smallest carboxylates  $HCOO^-$  and  $CH_3COO^-$ ,  
 595 the  $\bar{U}^{iw}(\infty)$  values are also almost insensitive to the fitting functions, as they differ by less  
 596 than 2 kcal mol<sup>-1</sup> on average. For these carboxylate ions, we may even note a much better  
 597 agreement among the  $\bar{U}^{iw}(\infty)$  values computed by not setting both  $a$  and  $\epsilon_1$  to zero. In this

598 case, their  $\bar{U}^{iw}(\infty)$  values differ only by about 1 kcal mol<sup>-1</sup> on average. For the largest  
 599 carboxylates ( $> \text{CH}_3\text{COO}^-$ ), the  $\bar{U}^{iw}(\infty)$  values are clearly more sensitive to the choice  
 600 of the fitting function. For them, the extrapolated values differ by about 5 kcal mol<sup>-1</sup> on  
 601 average. Hence, our extrapolation protocol to estimate the ion/water interaction energies in  
 602 liquid water appears to be robust enough only for small ions, regardless of their nature while  
 603 for large ions, in particular with a long linear alkyl chain, this protocol provides only a crude  
 604 estimate of the latter interaction energy, at least when considering the present droplet sizes.  
 605 Nevertheless, we note that the  $\bar{U}^{iw}(\infty)$  values for all the alkylcarboxylates are more stable  
 606 than the  $\text{CH}_3\text{NH}_3^+$  one by about 20% (25 kcal mol<sup>-1</sup>), regardless of the fitting function used.

607 The water destabilization energy values,  $\Delta\bar{U}_{\text{bulk}}^{ww}$ , are constant within 1 kcal mol<sup>-1</sup> for both  
 608 the cations and the anions. However, these energies are stronger by 35% for the carboxylates  
 609 than for the ammonium ions and  $\text{K}^+$  (that represents a difference in  $\Delta\bar{U}_{\text{bulk}}^{ww}$  around 13 kcal  
 610 mol<sup>-1</sup>). Hence, carboxylates affect more strongly the water structure in their vicinity than  
 611 ammonium and  $\text{K}^+$  ions. This stronger solvent destabilization induced by carboxylates leads  
 612 to cancel out most of the differences in the ion/water interaction energies  $\bar{U}^{iw}(\infty)$  between  
 613 carboxylates and the latter cations. Hence, as experimentally reported [50, 52, 53], our  
 614 simulation results show that the single ion absolute solvation enthalpies  $\Delta H_{g \rightarrow aq}$ , computed  
 615 according to

$$\Delta H_{g \rightarrow aq} = \bar{U}^{iw}(\infty) + \Delta\bar{U}_{\text{bulk}}^{ww} + \Delta\bar{U}_{\text{intra}}^{\text{ion}} - k_B T, \quad (16)$$

616 are all very close within a few kcal mol<sup>-1</sup> for the smallest ions  $\text{HCOO}^-$ ,  $\text{CH}_3\text{COO}^-$ ,  $\text{NH}_4^+$ ,  
 617  $\text{CH}_3\text{NH}_3^+$ , and  $\text{K}^+$ . These computed enthalpies are slightly overestimated on average, relative  
 618 to experiment, by about 2.5 kcal mol<sup>-1</sup> (see Table II). However for  $\text{CH}_3\text{COO}^-$ , our  $\Delta H_{g \rightarrow aq}$   
 619 value is in better agreement with experiment (about -90 kcal mol<sup>-1</sup> [19, 20, 52]) than the  
 620 values reported in previous theoretical studies that predicted: -80 kcal mol<sup>-1</sup> [19, 24] and  
 621 -87 kcal mol<sup>-1</sup> [20] by using pairwise forcefields, and -87 kcal mol<sup>-1</sup> [24] with a polarizable  
 622 forcefield. Nevertheless, for larger carboxylates, our  $\Delta H_{g \rightarrow aq}$  estimates differ more noticeably  
 623 compared to experimental values, from about 5 to 10 kcal mol<sup>-1</sup>. As already discussed above,  
 624 the extrapolation schemes we used appear to be not robust enough for large carboxylates,  
 625 which prevents us to further discuss the discrepancies between simulated and experimental  
 626  $\Delta H_{g \rightarrow aq}$  values.

627 To assess the accuracy of our computational protocol to model the carboxylate hydra-  
 628 tion, we may also consider the proton absolute solvation enthalpy  $\Delta H_{g \rightarrow aq}(\text{H}^+)$ , derived

629 from the experimental data summarized in Table I, the experimental carboxylate single-ion  
 630 solvation energies from Ref. [52] or the present computed values, according to the following  
 631 thermochemical cycle

$$\Delta H_{g \rightarrow aq}(\text{H}^+) = \Delta H_{g \rightarrow aq}(\text{BH}) + \Delta H_{aq, \text{dissociation}}^0(\text{BH}) - \Delta H_{g \rightarrow aq}(\text{B}^-) + \Delta H_g^{\text{prot}}(\text{B}^-) \quad (17)$$

632 Because of the lack of thermochemical data for hexanoate, we consider for it the same  
 633 experimental data as for pentanoate. When using our simulation results, the carboxylate-  
 634 based values  $\Delta H_{g \rightarrow aq}(\text{H}^+)$  range mainly between 257 and 270 kcal mol<sup>-1</sup>. These values are  
 635 clearly underestimated compared to the well-accepted experimental range of values, 271-275  
 636 kcal mol<sup>-1</sup> [44, 45, 54], and to the value corresponding to the experimental carboxylate  
 637 single solvation energies summarized in Table II,  $271.5 \pm 0.2$  kcal mol<sup>-1</sup>.

638 However, by considering only the data of the smallest carboxylates HCOO<sup>-</sup> and CH<sub>3</sub>COO<sup>-</sup>,  
 639 *i.e.* the ones for which the extrapolated values  $\bar{U}^{iw}(\infty)$  appear to be the most reliable, we  
 640 note then a better agreement between the theoretical and the experimental  $\Delta H_{g \rightarrow aq}(\text{H}^+)$   
 641 estimates. In particular, by considering the data computed from non-zero parameters  $a$   
 642 and  $\epsilon_1$ , the mean  $\Delta H_{g \rightarrow aq}(\text{H}^+)$  value is around 269 kcal mol<sup>-1</sup> for these small carboxylates.  
 643 That value corresponds to the lower limit of the experimental estimates and it agrees with  
 644 the value computed from methylated ammonium data, around 272 kcal mol<sup>-1</sup>. As already  
 645 mentioned, we computed the water destabilization energies  $\Delta \bar{U}_{\text{bulk}}^{ww}$  in our previous study [35]  
 646 dealing with ammonium ions from simulations performed using classical Ewald summation  
 647 techniques for neat water and the Particle Mesh Ewald method for ionic solutions. The  
 648 values reported in Table II are computed by comparing results computed using the same  
 649 Ewald protocol, which explains the small difference between the value reported here for the  
 650 cation-based  $\Delta H_{g \rightarrow aq}(\text{H}^+)$  and the previous one (270.6 kcal mol<sup>-1</sup>).

651 The short-range stabilizing carboxylate/water interactions are modeled by considering  
 652 two energy terms, namely  $U^{\text{disp}}$  and  $U^{\text{shb}}$ , for which it is not obvious to evaluate the correct  
 653 ratio, as well as the strength of the anti-cooperative character of  $U^{\text{shb}}$ . In particular, the  
 654 amount of destabilizing energy due to the anti-cooperative component of  $U^{\text{shb}}$  is about 7 kcal  
 655 mol<sup>-1</sup> for the HCOO<sup>-</sup>/ $N_w = 1000$  droplet system. Hence, a slightly more anti-cooperative  
 656  $U^{\text{shb}}$  carboxylate/water energy term may destabilize the carboxylate  $\Delta H_{g \rightarrow aq}$  by a few more  
 657 kcal mol<sup>-1</sup>, leading then to a better agreement between experiment and small carboxylate  
 658 simulation-based data for the proton solvation enthalpy. However, because of the uncertainty



659 tied to the protocol we used to extrapolate bulk ion/water interaction energies from droplet  
660 simulations, especially for large carboxylates, data corresponding to droplet systems much  
661 larger than the ones considered here might also help to further discuss this particular point.

#### 662 IV. CONCLUSIONS

663 We presented simulations concerning six linear alkylated carboxylates (from methanoate  
664 to hexanoate) solvated in water droplets comprising from  $N_w = 50$  to 1000 water molecules  
665 and in bulk water, as well as interacting at the air/liquid water interface. The simulation  
666 protocol is based on a polarizable model including, in particular, a specific short-range many-  
667 body anisotropic energy term to accurately model the ion/water interactions. The results  
668 show that all the carboxylates have a strong propensity for the air/water interface in the  
669 case of small droplet systems ( $N_w < 300$ ) while only carboxylates larger than propanoate  
670 have a noticeable propensity for the air/water interface in larger water droplets and at the  
671 air/liquid water interface. This is in line with recent experimental results [15]. However,  
672 as our simulations neglect acid/base phenomena, to further compare our results concerning  
673 the behavior of carboxylates at the air/water interface to experiment, a similar theoretical  
674 study of the solvation of neutral carboxylic acid needs to be performed.

675 Concerning carboxylate/water interactions, our calculations for 600 water droplets for  
676 example show that transferring an ion from the solution to the air/water interface is more  
677 endothermic for hexanoate than for ethanoate by 4 kcal mol<sup>-1</sup>. Nevertheless, ethanoate  
678 remains in the solution while hexanoate is on the surface. This implies a positive entropy  
679 change for moving the ion to the surface, by at least 3.3 cal mol<sup>-1</sup> K<sup>-1</sup> per CH<sub>2</sub> group.  
680 Both the enthalpy and entropy effects are consistent with the loss of the structure-making  
681 effects of the alkyl chain by removal from solution. The largest factor in this effect is the  
682 difference in hydrocarbon/water dispersion energy, which is more negative for hexanoate  
683 than ethanoate by 12 kcal mol<sup>-1</sup>, *i.e.* each CH<sub>2</sub> group contributes 3 kcal mol<sup>-1</sup> to the ion-  
684 water dispersion enthalpy. Further, comparable effects of alkyl groups were observed in the  
685 solvation of methylated ammonium ions, suggesting that the ionic head-groups and alkyl  
686 substituents are solvated as independent solutes.

687 As already reported for methylated ammonium ions and for K<sup>+</sup> [35], the present results  
688 show also that the ion/water polarization forces are centrifugal while the ion/water disper-

689 sion and Coulombic forces are centripetal in carboxylate/water droplets. Together, all of  
690 these results show the propensity of an ion for aqueous interfaces (regardless of whether it  
691 is a monoatomic cation or an alkylated cation or anion) to result from a complex interplay  
692 of microscopic forces, like the above-mentioned three ones. That also demonstrates the ne-  
693 cessity for explicitly and accurately accounting for ion/water polarization effects to perform  
694 reliable simulations of an ion interacting close to an aqueous interface, as already discussed  
695 by several authors [28–30].

696 The obtained carboxylate/droplet data allow us also to extrapolate the single carboxylate  
697 absolute solvation enthalpies and thus to estimate the proton absolute solvation enthalpy. By  
698 considering the data concerning the smallest carboxylates (methanoate and ethanoate), the  
699 present carboxylate-based proton solvation enthalpy is about  $269 \text{ kcal mol}^{-1}$ , a value in good  
700 agreement with the experimental one (ranging from  $271$  to  $275 \text{ kcal mol}^{-1}$ ) and the value  
701 that we reported using the same computational protocol for methylated ammonium ions [35]  
702 (about  $271 \text{ kcal mol}^{-1}$ ). For the largest carboxylate ions, the droplet data yield a proton  
703 solvation enthalpy largely underestimated, up to  $10 \text{ kcal mol}^{-1}$ , relative to experiment. To  
704 our opinion, that results mainly from the data set we used, which corresponds to droplet  
705 systems still too small (in particular, when we compare the droplet size to the size of the  
706 largest carboxylates like pentanoate and hexanoate). That can prevent us to extrapolate  
707 reliable results by using simple power-law functions of the droplet size as done here. This  
708 point needs thus to be further discussed, in particular by considering new results concerning  
709 larger ion/droplet systems (including around  $10\,000$  water molecules and more). Such  
710 simulations are still computationally demanding even by using forcefield-based approaches.  
711 Nevertheless, they will provide important informations allowing one to better quantify the  
712 impact of enthalpic effects (like the electrostatic interactions between water and an ionic  
713 head) and of entropic ones (which mainly drive the hydration of small hydrophobic solutes  
714 [48]) on the hydration properties of organic ions.

## 715 **SUPPORTING INFORMATION AVAILABLE**

716 Full description of the quantum computations, of the model parameter assignment strat-  
717 egy, of the molecular dynamics details and of data mentioned in the text. This material is  
718 available free of charge via the Internet at <http://pubs.acs.org>.

## ACKNOWLEDGMENTS

720 We thank Othman Bouizi and Emmanuel Oseret (Exascale Computing Research Labora-  
721 tory, a joint INTEL/CEA/UVSQ/GENCI laboratory) for their help in optimizing the code  
722 POLARIS(MD). We acknowledge an access to the supercomputing systems of the CCRT  
723 (Centre de Calcul et de Recherche Technologique) of the French Nuclear Agency (CEA),  
724 and the use of the Stampede supercomputing system at TACC/UT Austin, funded by NSF  
725 award OCI-1134872.

- 
- 726 [1]  
727 [2] Finlayson-Pitts, B. J. *Chemical Reviews* **2003**, *103*, 4801-4822.  
728 [3] Finlayson-Pitts, B. J. *Phys. Chem. Chem. Phys.* **2009**, *11*, 7760-7779.  
729 [4] Warshel, A.; Sharma, P. K.; Kato, M.; Xiang, Y.; Liu, H.; Olsson, M. H. M. *Chemical*  
730 *Reviews* **2006**, *106*, 3210-3235.  
731 [5] Jungwirth, P.; Winter, B. *Annual Review of Physical Chemistry* **2008**, *59*, 343-366.  
732 [6] McGorty, R.; Fung, J.; Kaz, D.; Manoharan, V. N. *Materials Today* **2010**, *13*, 34 - 42.  
733 [7] Mishra, H.; Enami, S.; Nielsen, R. J.; Stewart, L. A.; Hoffmann, M. R.; Goddard, W. A.;  
734 Colussi, A. J. *Proceedings of the National Academy of Sciences* **2012**, *109*, 18679-18683.  
735 [8] Prisle, N. L.; Raatikainen, T.; Laaksonen, A.; M., B. *Atmos. Chem. Phys.* **2010**, *10*, 5663-  
736 5683.  
737 [9] Gojlo, E.; Śmiechowski, M.; Panuszko, A.; Stangret, J. *The Journal of Physical Chemistry*  
738 *B* **2009**, *113*, 8128-8136.  
739 [10] Kameda, Y.; Ebata, H.; Usuki, T.; Uemura, O.; Misawa, M. *Bull. Soc. Chem. Jpn.* **1994**,  
740 *67*, 3159-3164.  
741 [11] Kameda, Y.; Mori, T.; Nishiyama, T.; Usuki, T.; Uemura, O. *Bull. Soc. Chem. Jpn.* **1996**,  
742 *69*, 1495-1504.  
743 [12] Kameda, Y.; Fukahara, K.; Mochiduki, K.; Naganuma, H.; Usuki, T.; Uemura, O. *J.*  
744 *Non-Cryst. Solids* **2002**, *312-314*, 433-437.  
745 [13] Rahman, H. M. A.; Hefter, G.; Buchner, R. *The Journal of Physical Chemistry B* **2012**,  
746 *116*, 314-323.

- 747 [14] Rahman, H. M. A.; Hefter, G.; Buchner, R. *The Journal of Physical Chemistry B* **2013**,  
748 *117*, 2142-2152.
- 749 [15] Ottosson, N.; Wernersson, E.; Soderstrom, J.; Pokapanich, W.; Kaufmann, S.; Svensson, S.;  
750 Persson, I.; Ohrwall, G.; Bjorneholm, O. *Phys. Chem. Chem. Phys.* **2011**, *13*, 12261-12267.
- 751 [16] Leung, K.; Rempe, S. B. *Journal of the American Chemical Society* **2004**, *126*, 344-351.
- 752 [17] Payaka, A.; Tongraar, A.; Rode, B. M. *The Journal of Physical Chemistry A* **2009**, *113*,  
753 3291-3298.
- 754 [18] Payaka, A.; Tongraar, A.; Rode, B. M. *The Journal of Physical Chemistry A* **2010**, *114*,  
755 10443-10453.
- 756 [19] Alagona, G.; Ghio, C.; Kollman, P. *Journal of the American Chemical Society* **1986**, *108*,  
757 185-191.
- 758 [20] Jorgensen, W. L.; Gao, J. *Journal of Physical Chemistry* **1986**, *90*, 2174-2182.
- 759 [21] Minofar, B.; Vácha, R.; Wahab, A.; Mahiuddin, S.; Kunz, W.; Jungwirth, P. *The Journal*  
760 *of Physical Chemistry B* **2006**, *110*, 15939-15944.
- 761 [22] Minofar, B.; Jungwirth, P.; Das, M. R.; Kunz, W.; Mahiuddin, S. *The Journal of Physical*  
762 *Chemistry C* **2007**, *111*, 8242-8247.
- 763 [23] Mahiuddin, S.; Minofar, B.; Borah, J. M.; Das, M. R.; Jungwirth, P. *Chemical Physics*  
764 *Letters* **2008**, *462*, 217 - 221.
- 765 [24] Meng, E. C.; Kollman, P. A. *The Journal of Physical Chemistry* **1996**, *100*, 11460-11470.
- 766 [25] Liang, T.; Walsh, T. R. *Phys. Chem. Chem. Phys.* **2006**, *8*, 4410-4419.
- 767 [26] Chang, T.-M.; Dang, L. X. *Chemical Reviews.* **2006**, *106*, 1305-1322.
- 768 [27] Jungwirth, P.; Tobias, D. J. *Chemical Reviews* **2006**, *106*, 1259-1281.
- 769 [28] Wick, C. D. *J. Chem. Phys.* **2009**, *131*, 084715.
- 770 [29] Wick, C. D.; Cummings, O. T. *Chem. Phys. Lett.* **2011**, *513*, 161-186.
- 771 [30] Netz, R. R.; Horinek, D. *Annu. Rev. Phys. Chem.* **2012**, *63*, 401-418.
- 772 [31] Simon, A.; Iftner, C.; Mascetti, J.; Spiegelman, F. *The Journal of Physical Chemistry A*  
773 **2015**, *119*, 2449-2467.
- 774 [32] Consta, S.; Oh, M. I.; Soltani, S. *International Journal of Mass Spectrometry* **2015**, *377*,  
775 557 - 567 Special Issue: {MS} 1960 to Now.
- 776 [33] Réal, F.; Vallet, V.; Flament, J.-P.; Masella, M. *J. Chem. Phys.* **2013**, *139*, 114502.

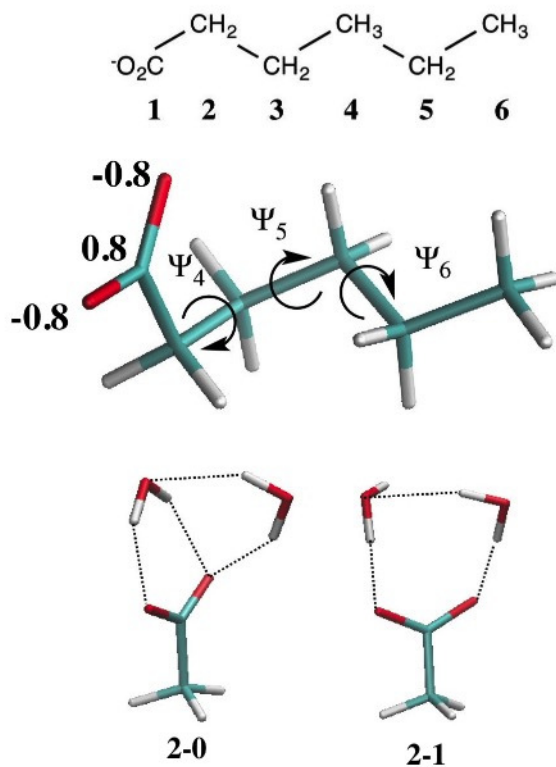
- 777 [34] Trumm, M.; Guerrero Martinez, Y. O.; Réal, F.; Schimmelpfennig, B.; Masella, M.; Val-  
778 let, V. *J. Chem. Phys.* **2012**, *136*, 044509.
- 779 [35] Houriez, C.; Meot-Ner (Mautner), M.; Masella, M. *The Journal of Physical Chemistry B*  
780 **2014**, *118*, 6222-6233.
- 781 [36] Saykally, R. *Nature Chemistry*. **2013**, *5*, 82-84.
- 782 [37] “Gaussian 09 Revision D.01”, Gaussian Inc. Wallingford CT 2009.
- 783 [38] Réal, F. personal communication.
- 784 [39] Thole, B. *Chem. Phys.* **1981**, *59*, 341-350.
- 785 [40] Brooks, B. *et al. J. Comput. Chem.* **2009**, *30*, 1545-1615.
- 786 [41] Allen, F. H. *Acta Crystallographica Section B* **2002**, *58*, 380-388.
- 787 [42] Kondo, T.; Miyazaki, Y.; Inaba, A.; Koga, Y. *The Journal of Physical Chemistry B* **2012**,  
788 *116*, 3571-3577.
- 789 [43] Ben-Amotz, D. *The Journal of Physical Chemistry Letters* **2015**, *6*, 1696-1701.
- 790 [44] Meot-Ner, M. *J. Phys. Chem.* **1987**, *91*, 417-426.
- 791 [45] Meot-Ner (Mautner), M. *Chem. Rev.* **2005**, *105*, 213-284.
- 792 [46] Caleman, C.; Hub, J.; van Maaren, P.; van der Spoel, D. *Proc. Natl. Acad. Sci. USA.* **2011**,  
793 *108*, 6838-6842.
- 794 [47] Dang, L. X.; Chang, T.-M. *J. Phys. Chem. B* **2002**, *106*, 235-238.
- 795 [48] Chandler, D. *Nature* **2005**, *437*, 640-647.
- 796 [49] Aue, D. H.; Webb, H. M.; Bowers, M. T. *Journal of the American Chemical Society* **1976**,  
797 *98*, 318-329.
- 798 [50] Meot-Ner, M.; Sieck, L. W. *Journal of the American Chemical Society* **1986**, *108*, 7525-7529.
- 799 [51] Peslherbe, G. H.; Ladanyi, B. M.; Hynes, J. T. *J. Phys. Chem. A* **1999**, *103*, 2561-2571.
- 800 [52] Wilson, B.; Georgiadis, R.; Bartmess, J. E. *Journal of the American Chemical Society* **1991**,  
801 *113*, 1762-1766.
- 802 [53] Meot-Ner (Mautner), M. *Chem. Rev.* **2012**, *112*, PR22-PR103.
- 803 [54] Tuttle, T. R.; Malaxos, S.; Coe, J. V. *J. Phys. Chem. A* **2002**, *106*, 925-932.

804

805

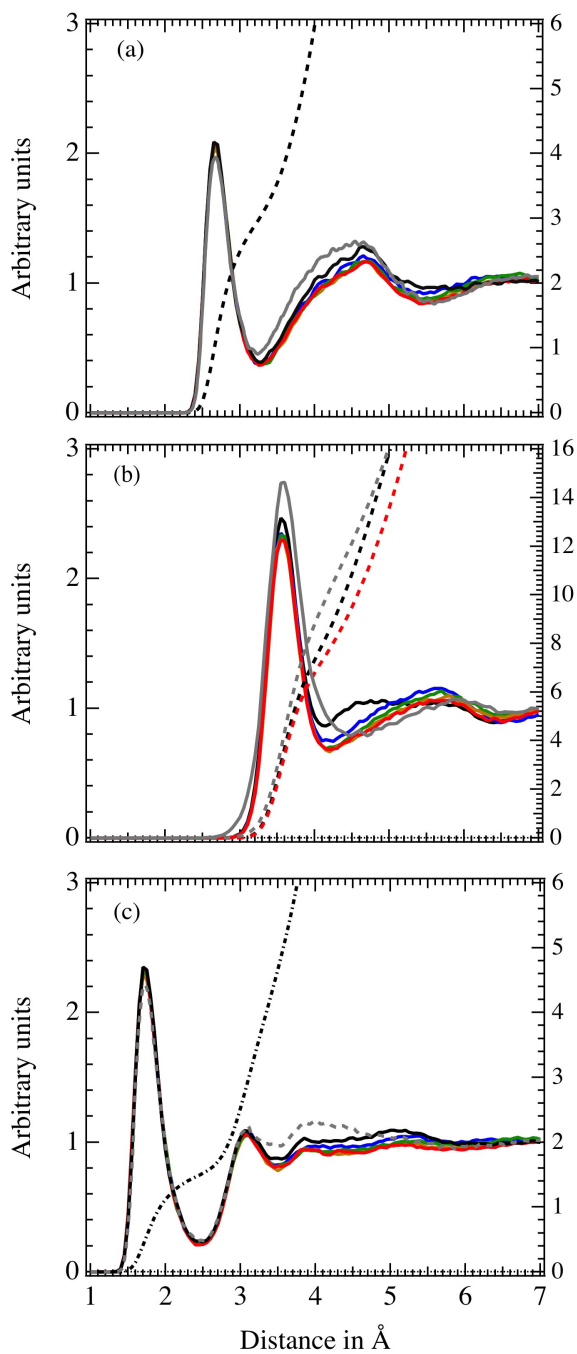
## FIGURES

806



807

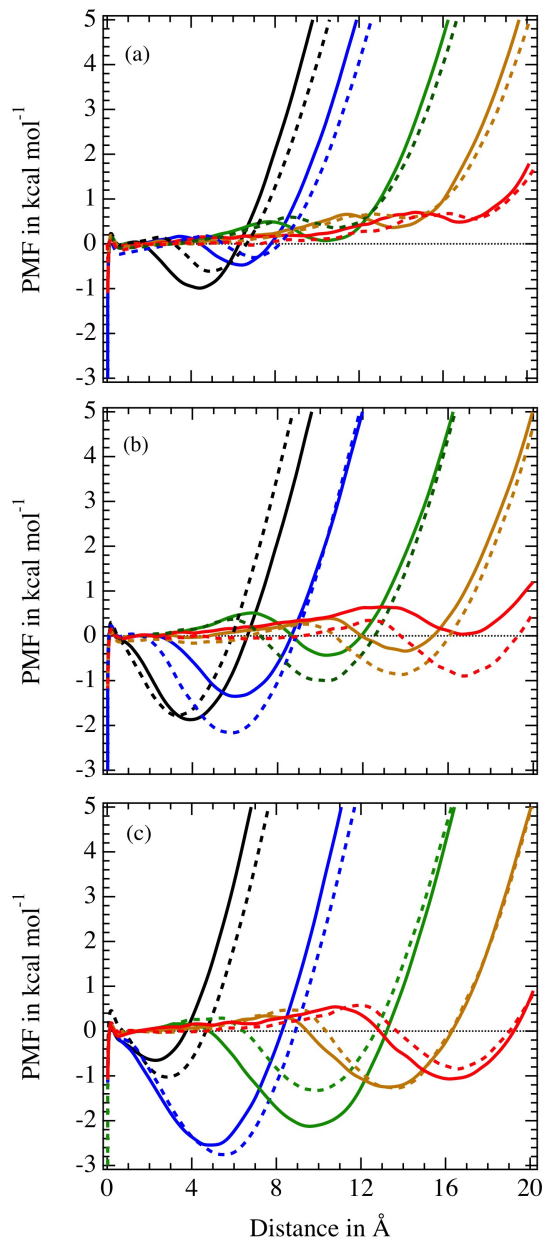
808 FIG. 1. Top: Labeling of carbon atoms in the carboxylates (bold characters). Middle: the most  
 809 stable structure of hexanoate (according to our model, the three dihedral angles  $\Psi_n$  are of 66.6,  
 810 49.6 and 177.8°, for  $n = 4-6$ , respectively). The numbers shown close to the hexanoate anionic  
 811 head are the model electrostatic charges, in  $e$ . Bottom: the two  $\text{CH}_3\text{COO}^-/(\text{H}_2\text{O})_2$  structures **2-0**  
 812 and **2-1**.



813

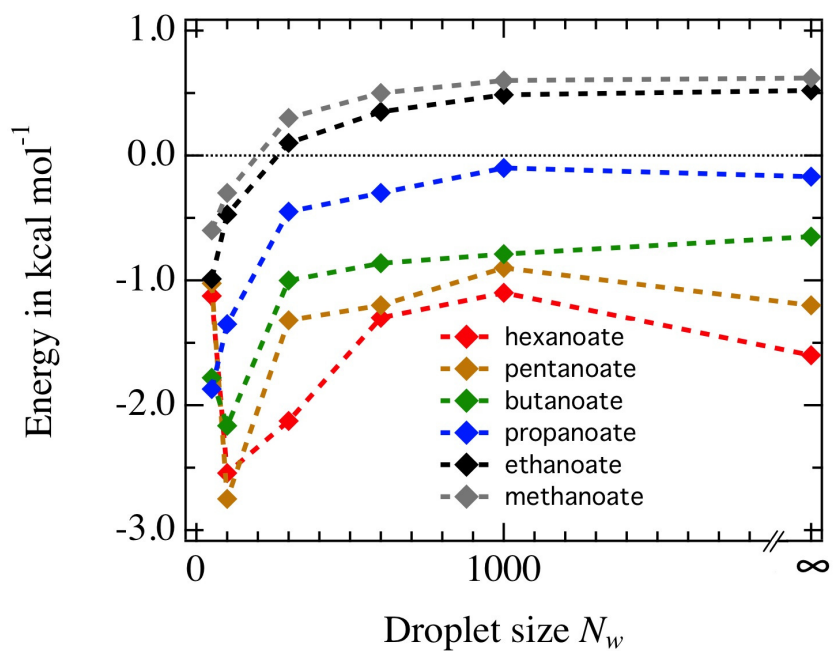
814 FIG. 2. Carboxylate/water radial distribution functions:  $g_{OO_w}$  (a),  $g_{CO_w}$  (b), and  $g_{OH_w}$  (c). Grey  
 815 line: methanoate; black: ethanoate; blue: propanoate; green: butanoate; orange: pentanoate; red:  
 816 hexanoate. Corresponding dashed lines: some examples of integrated radial distribution functions.  
 817  $g_{OO_w}$  and  $g_{OH_w}$  are averaged over the carboxylate oxygen atoms and the water hydrogen atoms.





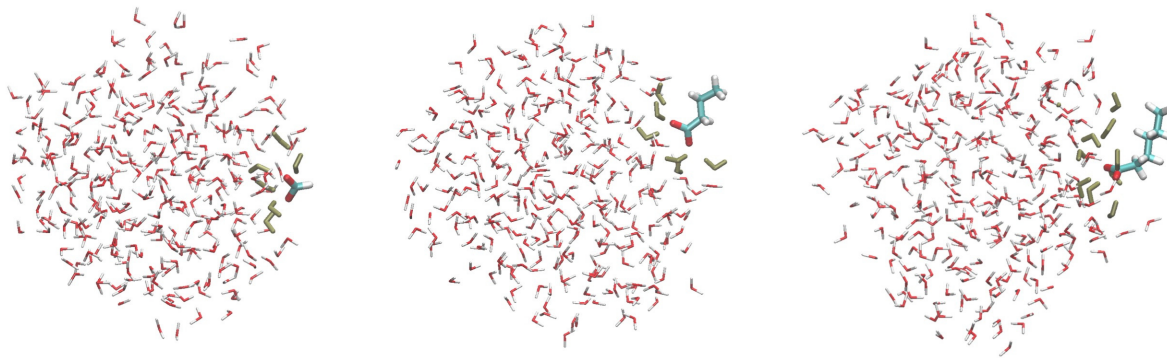
818

819 FIG. 3. Carboxylate/water droplet PMF. (a):  $\text{HCOO}^-$  (—) and  $\text{CH}_3\text{COO}^-$  (- -); (b):  $\text{C}_2\text{H}_5\text{COO}^-$   
 820 (—) and  $\text{C}_3\text{H}_7\text{COO}^-$  (- -); (c):  $\text{C}_4\text{H}_9\text{COO}^-$  (—) and  $\text{C}_5\text{H}_{11}\text{COO}^-$  (- -). Black:  $N_w = 50$ ; blue:  
 821  $N_w = 100$ ; green:  $N_w = 300$ ; orange:  $N_w = 600$ ; red:  $N_w = 1000$ .



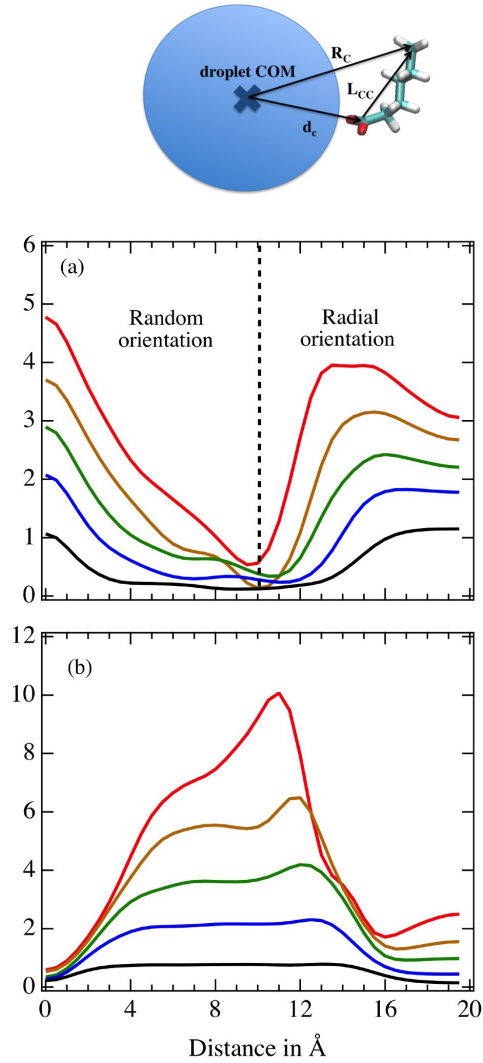
822

823 FIG. 4. PMF values at the minimum close to the air/droplet interfaces as a function of the droplet  
 824 size. The bulk values ( $\infty$ ) are computed from air/liquid water simulations and by accounting for  
 825 the corrections  $\delta$ PMF (see Equation 11).



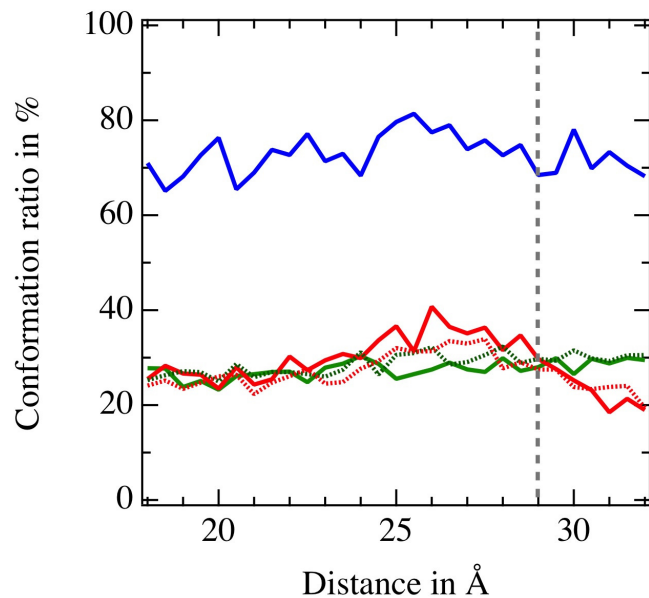
826

827 FIG. 5. Some simulation snapshots showing representative structures corresponding to the PMF  
828 minimum values close to the droplet boundary. Methanoate, butanoate and hexanoate, respec-  
829 tively, interacting with a  $N_w = 300$  droplet. The water molecules of the first hydration shell of the  
830  $\text{COO}^-$  moiety are shown in green.



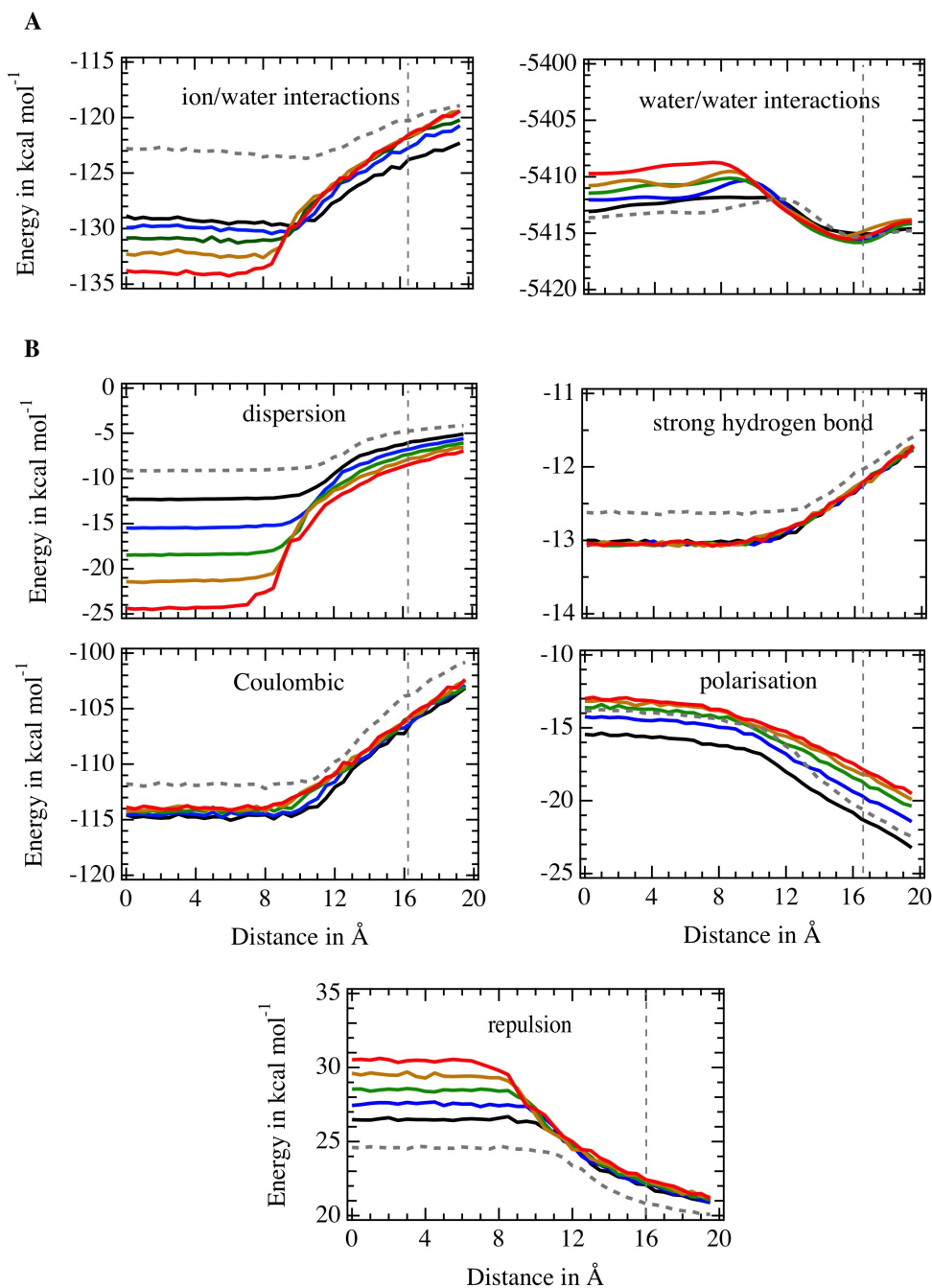
831

832 FIG. 6. Top: Definition of the geometric parameters  $R_C$ ,  $d_c$  and  $L_{CC}$ . Middle and bottom:  $\Delta R_C$   
 833 (a) and  $\delta R_C$  (b) quantities plotted as a function of  $d_c$ , for  $N_w = 1000$  droplet systems. Black:  
 834 ethanoate; blue: propanoate; green: butanoate; orange: pentanoate; red: hexanoate. The  $L_{CC}$   
 835 values in gas phase are 1.5, 3.3, 3.9 and 4.9  $\text{\AA}$ , from ethanoate to hexanoate, respectively.



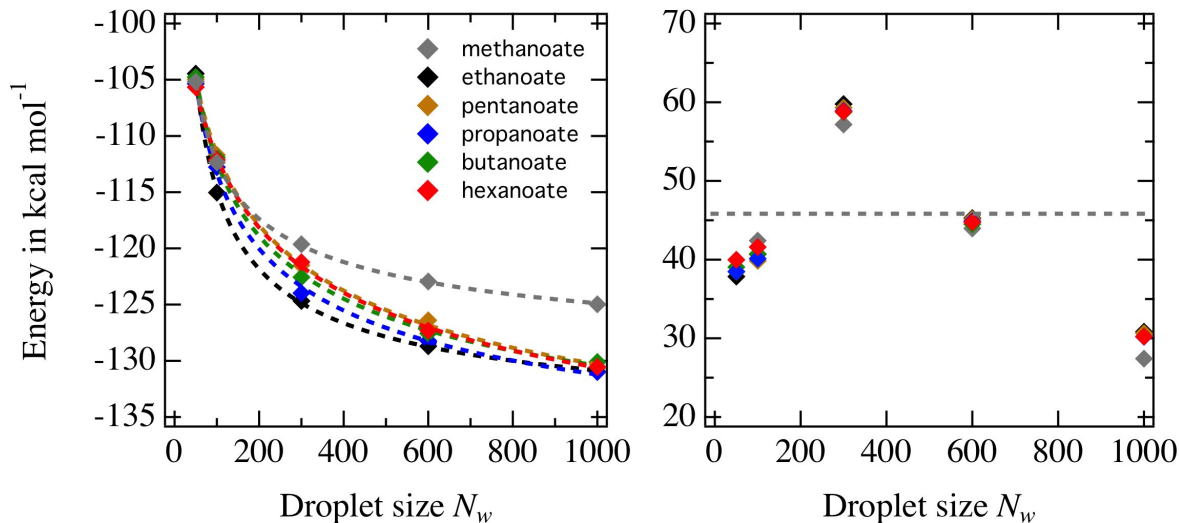
836

837 FIG. 7. Anti/gauche ratio for the conformations of the dihedral angles  $\Psi_{n=4,5,6}$  for hexanoate (full  
 838 line) and  $\Psi_{n=4,5}$  for pentanoate (dashed line), as a function of  $d_c$ , for air/liquid water interface  
 839 simulations. Red:  $\Psi_4$ ; green:  $\Psi_5$ ; blue:  $\Psi_6$ . The vertical dashed line indicates the position of the  
 840 air/liquid water interface.



841

842 FIG. 8. **A**: Ion/water and water/water microscopic energies as a function of the ion location  
 843 for a  $N_w = 600$  droplet. For water/water interactions, the original data are smoothed using a  
 844 binomial filter to reduce the noise due to evaporation effects. **B**: Components of the ion/water  
 845 interaction energies. Dashed grey line: HCOO<sup>-</sup>; black line: CH<sub>3</sub>COO<sup>-</sup>; blue: C<sub>2</sub>H<sub>5</sub>COO<sup>-</sup>; green:  
 846 C<sub>3</sub>H<sub>7</sub>COO<sup>-</sup>; orange: C<sub>4</sub>H<sub>9</sub>COO<sup>-</sup>; red: C<sub>5</sub>H<sub>11</sub>COO<sup>-</sup>. The vertical dashed line indicates the  
 847 position of the droplet interface.



848

849 FIG. 9. Mean ion/water interaction (left) and water destabilization (right) energies as a func-  
 850 tion of the droplet size. For ion/water energies, the power-law fitting functions corresponding  
 851 to  $(a, \epsilon_1)$  different from  $(0, 0)$  are shown in dashed lines. For water destabilization energies, the  
 852 horizontal dashed grey line corresponds to the mean bulk water destabilization energy. Compared  
 853 to methylated ammonium ions, the droplet water destabilization energies appear to be closer in  
 854 magnitude for all the carboxylates, however, they behave similarly, i.e., they reach a maximum for  
 855  $N_w = 300$  and then they decrease well below the bulk values. Note that the uncertainty affecting  
 856 the water destabilization energies due to evaporation phenomena is around  $\pm 5$  kcal mol<sup>-1</sup>.





857

## **TABLES**

858

Carboxylate	$\Delta H_g^{prot}$	$\Delta H_{g \rightarrow aq}^{BH}$	$\Delta H_{aq, dissociation}^0$
HCOO <sup>-</sup>	-345.3	-11.5	-0.04
CH <sub>3</sub> COO <sup>-</sup>	-348.5	-12.7	-0.10
C <sub>2</sub> H <sub>5</sub> COO <sup>-</sup>	-347.5	-14.6	-0.14
C <sub>3</sub> H <sub>7</sub> COO <sup>-</sup>	-346.5	-17.4	-0.69
C <sub>4</sub> H <sub>9</sub> COO <sup>-</sup>	-346.2	-19.9	-0.70

859 TABLE I. Thermochemistry of carboxylate protonation and solvation.  $\Delta H_g^{prot}$ : carboxylate pro-  
860 tonation enthalpy in gas phase.  $\Delta H_{g \rightarrow aq}^{BH}$ : absolute solvation enthalpy of a protonated carboxylate.  
861  $\Delta H_{aq, dissociation}^0$ : proton dissociation enthalpy in aqueous phase of a protonated carboxylate. All  
862 enthalpy data at room temperature and pressure, in kcal mol<sup>-1</sup>, from Ref. 45.

863

	$-\Delta\bar{U}^{iw}(\infty)$				$\Delta\bar{U}_{\text{ww}}$	$\Delta\bar{U}_{\text{intra}}$	$-\Delta H_{g\rightarrow aq}$	$\Delta H_{g\rightarrow aq}(\text{H}^+)$
	(0,0)	(a,0)	(0, $\epsilon_1$ )	(a, $\epsilon_1$ )				
$\text{HCOO}^-$	136.0	133.6	133.3	133.6	46.4	0.0	87.7 (85.3)	269.1
$\text{CH}_3\text{COO}^-$	146.4	140.2	138.4	140.1	47.4	0.8	92.0 (89.7)	269.0
$\text{C}_2\text{H}_5\text{COO}^-$	145.7	147.3	147.3	145.0	46.4	0.3	100.5 (90.5)	261.7
$\text{C}_3\text{H}_7\text{COO}^-$	145.7	148.3	148.3	135.6	46.6	0.7	98.3 (92.9)	266.3
$\text{C}_4\text{H}_9\text{COO}^-$	143.7	155.7	151.7	155.6	46.5	1.0	107.4 (95.2)	259.4
$\text{C}_5\text{H}_{11}\text{COO}^-$	143.6	158.1	152.7	157.0	47.7	1.2	107.6 (-)	259.2
$\text{NH}_4^+$	122.2	124.4	124.1	124.4	35.3	0.0	89.0	273.0
$\text{CH}_3\text{NH}_3^+$	113.6	115.7	115.5	114.1	34.4	0.1	80.8	272.3
$(\text{CH}_3)_2\text{NH}_2^+$	106.4	104.9	104.8	102.4	33.4	0.3	70.3	269.0
$(\text{CH}_3)_3\text{NH}^+$	100.3	103.6	103.2	101.2	32.3	0.2	70.2	276.0
$\text{K}^+$	119.6	120.1	120.1	116.1	30.5	-	88.3	

864 TABLE II. Extrapolated ion/water energies  $\Delta\bar{U}^{iw}(\infty)$ , differences in ion intramolecular defor-  
865 mation energies  $\Delta\bar{U}_{\text{intra}}$  and in water destabilization energies  $\Delta\bar{U}_{\text{ww}}$  due to the presence of the  
866 ion in water, single ion solvation enthalpies  $\Delta H_{g\rightarrow aq}$ , and absolute proton solvation enthalpies  
867  $\Delta H_{g\rightarrow aq}(\text{H}^+)$ . The four values for  $\Delta\bar{U}^{iw}(\infty)$  correspond to the data extrapolated using different  
868 fitting functions, whose parameters  $a$  and/or  $\epsilon_1$  are set to zero or taken as adjustable.  $\Delta H_{g\rightarrow aq}$   
869 and  $\Delta H_{g\rightarrow aq}(\text{H}^+)$  values are averaged from  $\Delta\bar{U}^{iw}(\infty)$  values obtained with parameters different of  
870 (0,0). For  $\Delta H_{g\rightarrow aq}$ , the experimental values for carboxylates cited in parentheses are taken from  
871 Ref. [52]. All energy data in kcal mol<sup>-1</sup>.